Department of the Navy
Office of Naval Research
Fluid Mechanics Branch
Contract N6onr-244, Task Order II
(NR 062-010)

EFFECT OF THE VOLUTE ON PERFORMANCE OF A CENTRIFUGAL PUMP IMPELLER

R. D. Bowerman

Hydrodynamics Laboratory
California Institute of Technology
Pasadena, California

Project Supervisor:
A. J. Acosta

Approved by:
A. Hollander

Report No. E-19.7
March 1955

ABSTRACT

An experimental study of volute influence on radial flow impeller performance was conducted by operating a single impeller with three different sets of volute vanes. In each case, over-all performance was measured and internal flow study within the volute was made. The results show that at their respective design flow rates the influence of the volutes is least and the deviation of performance from the free impeller operation is small. At off-design flow rates there are major changes in the impeller performance due to the presence of the volutes. Large real fluid effects, coupled with a quite nonuniform velocity pattern at the impeller exit, result in a flow through the volute that does not resemble a potential flow. Even so, the fluid losses through the volute are comparatively small. It is also shown that at off-design conditions, the flow cannot be irrotational and therefore potential flow theories cannot be used in describing the flow or predicting performance.

CONTENTS

I. INTRODUCTION

The pump research program of the Hydrodynamics Laboratory of the California Institute of Technology has been directed towards determining basic design information by systematically studying the performances of pump components and by correlating performance with internal flow phenomena. Previously extensive work has been conducted on centrifugal impellers operated with a vaneless diffusor, i.e., an annular passage of constant breadth. Thus, polar symmetric conditions existed for the impeller over the complete range of flow rates. An impeller operated in this manner is herein termed a free impeller. In the present work, effects of the volute case on the aggregate pump have been studied by successively combining three simplified two-dimensional volute shapes with a single impeller (previously studied as a free impeller) and conducting over-all performance and internal flow experiments on the combinations.

The information sought can be roughly divided into two categories: (1) the over-all performance for comparison of the different impeller-volute combinations and determination of the volute effect on the impeller itself; and (2) the nature of the flow through the volute, its agreement with potential theory and its correspondence with the features of the over-all performance. At a given speed of rotation, the over-all performance is described completely by the head and torque as functions of flow rate from which the water power and efficiency can be calculated. The flow in the volute is determined by measurements of the total head and static head distributions from which velocity can be calculated.

With regard to the over-all performance of the impeller-volute combinations, a distinction is made between impeller performance based on averaged head measurements made at the impeller exit and pump performance based on averaged head measurements made at the volute exit. Furthermore, as the above definition of pump performance indicates, the "pump" of this test is not directly comparable to a commercial pump, as the latter also includes final collection of the discharge into a single pipe with the consequent additional adjustment of the flow pattern to uniform pipe flow. Thus the complete pump is subject to additional mixing losses which are not accounted for in the volute losses reported here. It should also be noted that unlike commercial tests, the torque due to disc friction and other mechanical losses is not included in the present tests.

II. DESIGN AND CONSTRUCTION

The impeller employed in the investigation was a two-dimensional design with a 20-degree inlet angle and a 23.5 degree outlet angle, and has been thoroughly described in previous publications.[1, 2, 3*] The two-dimensional volute cases were formed by fitting the volute vanes between parallel diffusor shrouds as seen in Figs. 1 and 2. Double volute construction was chosen to meet space limitations and to make an added study of flow symmetry. It should be noted that the volute vanes extend inward quite close to the impeller vanes. This close proximity is not common in commercial designs; however, for the purposes of this study, the maximum effect of the volutes was desired.

The volute vane shapes were derived by considering the elementary theory of constant angular momentum. In two-dimensions this yields the equation of the familiar logarithmic spiral,**

$$r_v = e^{\frac{\phi_x \eta_x}{\psi_x}\theta}$$

where r_v and θ are the radial and angular coordinates of the volute vane, ϕ and ψ are dimensionless coefficients of the flow rate and head, respectively, and η is the efficiency.*** Calculation of a volute shape was made by choosing a volute design flow rate ϕ_x and taking the corresponding ψ_x and η_x data from the free impeller characteristics. The ratio $\phi_x \eta_x / \psi_x$ which is the tangent of the volute vane angle is also the tangent of the actual flow discharge angle from the impeller at the chosen flow rate. The three sets of volutes resulted from the choice of ϕ_x equal to 75%, 100%, and 120% of the free impeller design point, ϕ_e. All pertinent dimensions and design constants are given in Appendix IV.

The volute vanes were formed of 1/8-in. aluminum sheet, 1.2 in. wide, bent to match metal templates cut to the r_v and θ coordinates. The vane leading edges were rounded. The templates were also used to scribe the vane positions on the diffusor shrouds and the vanes were held in position with numerous small brass screws. A single set of shrouds was made to accommodate all three sets of vanes.

---

*Numbers refer to references at the end of the report.
**See Appendix II for derivation.
***Also see Appendix I, Notation.

III. EXPERIMENTAL WORK

1. Test Program

The following experiments were made on each of the impeller-volute combinations:

I. Static head measurements around the impeller periphery.
II. Total head measurements at the radial probe stations in the volute passage. Total head measurements were made at five elevations.
III. Input torque measurements.

Two supplementary experiments were made on the 100% volute:

IV. Static head distribution on the volute vanes.
V. Tuft studies - 3/8 in. streamers suspended in the volute passages.

2. Instrumentation

The general laboratory facilities have been thoroughly described in previous publicaations[1, 2] and a schematic diagram is shown in Fig. 3. The supply pump and throttle valve regulate the flow which is measured by any one of the three venturi meters. Mercury manometers are used to measure the pressure difference across the venturis. Flow rate settings are usually accurate to one-half percent or better. The test pump operates submerged in an open basin, thus permitting easy access to test equipment. The pump is driven by a 1/2 hp d.c. motor mounted as a dynamometer and equipped with a speed control unit which permits repeated speed settings with the speed held to within one-tenth rpm during operation.

The arrangement for taking the radial position data of test II involved slotting the top lucite shroud at 60 degree intervals to receive brass inserts of which one group were drilled for static taps and another group drilled to hold total head probes (Fig. 1b, 2b). Care was taken to have the inserts flush with the inner surface. The total head tubes used were slightly unusual in design, and their dimensions and calibration are presented in Fig. 5. The angular direction and elevation of the probes were maintained by pouring melted wax around the base of the probes. For test I, 42 static taps (0.020 in. diameter holes drilled in the top shroud) were spaced around the impeller periphery 3/16 in. from the impeller exit. The static taps of test IV were

located in the top shroud 1/32 in. from the volute vanes, closely spaced on either side of the tongue, with a few placed along the full extent of the inside of the vanes. Locations of all piezometer taps are shown in Fig. 1b.

All head measurements were referenced to the total head at the inlet of the impeller. The use of two multitube manometers permitted as many as 60 simultaneous readings which allowed rapid collection of the data (Fig. 4).

Torque measurement was accomplished by balancing the reaction torque of the motor case with weights suspended over a pulley from a lever arm. The balance position was indicated by a Statham displacement gage and fixed bridge circuit.

3. Procedure

All tests were conducted at 150 rpm over an established set of flow rates. To minimize the effect of probe interference, all static head data were taken independently of the total head data and total head data were taken with the probes evenly divided between the two volute passages to maintain flow symmetry.

The torque tests required careful technique as the bridge drift and general laboratory vibration contributed to wide scatter in the readings. As the torques involved at the low rpm were small (0.2-0.5 ft-lb), the percentage error was large. Continual checks were made on the bridge zero and statistical methods were applied to the taking of each reading. As only the torque due to the impeller vane action was wanted, the tare torque which included the motor windage and the fluid disc friction on the outside of the impeller, had to be taken. This was done by running the impeller empty but with a temporary basin holding water atop the impeller. Simulation of actual running conditions was difficult and the reading was sensitive, but identical technique was employed for all the torque tests. Estimated final torque error is within $\pm$ 2 percent.

The tuft studies were conducted simply by gluing thread streamers to the bottom shroud and suspending from needles other streamers successively at four elevations in the passage. The flow patterns were then photographed.

IV. RESULTS AND DISCUSSION

1. Presentation of Data

All quantities are reported as dimensionless coefficients as defined under notation. The curves of Fig. 10 represent the impeller head as a function of the angular position from the volute tongue. The overall impeller head is the average of the data of Fig. 10 and it should be recognized that these averages cannot be accurate where the curves differ widely. The overall pump head (Fig. 14) was obtained by an integrated average of the head values over the volute exit. Velocity coefficients were calculated from the total head-static head difference wherein it was necessary to assume that the static head at the top shroud was a representative of that across the passage depth.

With regard to free impeller head values, some explanation is required as to the manner in which they were obtained. In Fig. 11, curves A and B are the result of earlier work on the impeller where curve A represents measurements made 1/16 in. away from the impeller vane exit and curve B, 3/8 in. away. The difference of these curves was considered in Ref. 1 wherein at low flow rates it was decided that large mixing losses occur immediately following the impeller exit. Values from curve A were used in calculating the volute shapes. The data for curve C were currently taken in an identical manner as the data with volutes, i.e., 5/32 in. away from the impeller exit. Curve C, generally in accord with curves A and B, is taken as the free impeller performance for comparison with the data of the volutes.

2. Effect of Volutes on Performance

A. Overall Results

The experimental results show that the volute shape is quite prominent in determining the performance characteristics of a pump. The significant result is that the performance is controlled by the influence of the volute shape on the impeller operation rather than by the addition of losses to the fluid within the volute. Conclusive evidence that the impeller operates differently with different volute shapes is found in the torque curves (Fig. 15). Although there is not too much difference in the torque curves at low flow rates, above ϕ equal to

0.09 the curves are distinct and at ϕ above 0.14 there is considerable variance. The 75% and 100% combinations generally require somewhat greater torque than the free impeller whereas the 120% combination torque requirement is about the same as the free impeller. The behavior of the torque curves is given further consideration in the Theoretical Remarks.

Additional evidence of volute effect on impeller performance is given by the impeller head curves (Fig. 12). The heads are similar over the span of the design points, however, at low flow rates and high flow rates, there are large differences in the head curves. In general it can be concluded that each volute causes different loss distribution within the impeller and immediately following it for the following reasons: At very low flow rates each of the four cases must have a different impeller loss because the heads are quite different even though there is little change in the torques. At high flow rates, the impeller heads of the 120%, 100% and 75% combinations successively decrease and are lower than the free impeller values; however, the torques progressively increase, all being as high or higher than the free impeller requirements. The impeller efficiency curves (Fig. 13) reflect the effect of these losses.

B. Effect of Volutes at Design Points

The operation of each volute impeller combination is optimum at approximately the individual volute design flow rate. The heads produced by the 100% and 120% combinations are almost the same as the free impeller head measured 5/32 in. away from the impeller exit. At the flow rate 0.75 ϕ_e, the free impeller head measured at 5/32 in. away is below that measured 1/16 in. away, and the 75% volute combination produced a head between these two free impeller values. Evidently in the 75% case, the presence of the volute alleviates the conditions causing the losses immediately following the impeller.

The internal flow data also support the fact that the volutes operate best at their design points. In each case, the radial surveys of total and static head and their consequent velocity distributions are smooth (Fig. 7 and 8), and the impeller total heads, measured at the various angular positions (Fig. 10) are nearly equal. The volute vane pressure distributions and the tuft studies of the 100% combination also show

"best" flow conditions at the design point.

Likewise the static pressure distribution around the impeller periphery is quite uniform (Fig. 6). These results indicate that the volute can be designed without taking into account the effect of friction at least for the relatively high Reynolds numbers (2.4×10^5) of these tests.

C. Complete Pump Performance

The pump performance curves (Figs. 14, 15, and 16) are seen to be not significantly different from the impeller performance curves. There are some losses as the fluid passes through the volute as demonstrated by the total head curves compared in Fig. 17. At the volute design points, the losses through the volutes in each case are approximately 3 percent of the total head of the impeller (which amounts to about 20 percent of the volute exit velocity head). However, except at the volute design flow rates, the losses incurred in the volute are of a lesser magnitude than the changes in impeller performance of the three volute combinations. All impeller-volute combinations have nearly equal best efficiency (about 87 percent) which is probably due to the fact that the design points of the volutes are within the high efficiency region of the free impeller. It is not likely that a volute designed below the high efficiency region of the impeller would give good performance.

3. Flow Patterns through the Volute

As happens in many other flow problems, the flow in the volute has an approximate potential flow static pressure distribution, but the velocity distribution is not at all that predicted by theory. The local total and static head curves and horizontal velocity profile plots (Figs. 7 and 8) show that at design points the velocity diminishes to some degree with increasing radius to about one-third of the volute passage width, and from there on to the volute vane it is nearly constant. Potential flow requires the velocity to diminish inversely as the radius. Furthermore, over the entire range of flow rates there appears to be a region of high velocity flow along the concave side of the volute vane that would not ordinarily be expected. It is believed that this result is due to a secondary flow of the high energy fluid coming from the impeller shroud boundary layer. Considerable flow disturbance is caused by this discharged impeller boundary layer as can be

seen in Figs. 7, 8, and 9. The effect is notably more pronounced on the bottom surface as the bottom impeller shroud has a larger diameter. The fluid elements with varying total energy necessarily mix at the impeller exit, and this process accounts for some of the observed losses. The presence of the volute tongue is responsible for local disturbances that further complicate the flow in the volute as seen in Fig. 19.

4. Miscellaneous Remarks

With regard to the double volute construction, differences in values measured in one volute half of the pump from the other half were observed, but no strong systematic differences were noted. There was apparently no instability of the flow and the differences resulted from the disposition and influence of the total head probes and of slight differences in construction. The 100% volute vanes were found to be slightly dissimilar, the results of which are evident in the vane static head distribution curves (Fig. 18). Similar measurements were taken on each volute half, and those curves not specifically showing the data of both halves of the pump are averages of the two.

In conjunction with the velocity calculations, a discrepancy in the data was discovered. An integration of velocity over the volute discharge area resulted in a value of flow rate coefficient ϕ that was approximately a constant amount too large. At the design points of the 75% and 100% combinations, the integration gave a value about 5 percent too high and about 8 percent too high for the 120% pump. This discrepancy is much larger than can be accounted for by experimental error. The only explanation that can be offered is that there was a possible systematic over-estimation in the process of the graphical integration of the velocity curves, since their absolute values are small. In any event, it is certain that all trends are correct even though there may be some question of absolute values.

V. THEORETICAL REMARKS

It would be of interest to be able to predict, roughly, the direction and magnitude of the volute-impeller interference effects. Early investigators, i.g., Straszacker,[4] have made attempts in this direction by assuming the absolute flow to be irrotational and inviscid, so that potential theory could be used. Straszacker was chiefly concerned with the flow and streamline picture at the impeller exit, rather than performance calculations.

It should be clear that at off-design conditions high velocities can occur at the volute tongue and these velocities may cause substantial deviations in the velocity pattern. Due to the presence of the volute, the absolute flow leaving the impeller may not be irrotational. In fact, if an infinite number of impeller vanes is assumed, then the head at each point around the impeller periphery will not be constant. This may be seen from the "general" Bernoulli equation in rotating coordinates, which gives for the impeller head

$$h = \frac{u_2 c_2 \cos \alpha_2 - u_1 c_1 \cos \alpha_1}{g} - \frac{u_2}{g \sin^2 \beta_2} \frac{dc_{m_2}}{d\theta} \ln \left(\frac{r_2}{r_1} \right)$$

where θ is the angular coordinate, β_2 is the blade angle, c the absolute velocity and r the radius. (This equation is derived in Appendix III). Since the flow approaching the impeller is presumed to be of constant total head, the leaving absolute flow cannot have constant energy according to the above equation. Thus the assumption of irrotational absolute flow can only be an approximation for this problem.

The volute influence on the impeller performance is considered as follows: Suppose that the radial velocity is given by

$$c_m = \bar{c}_m + c'_m$$

and the tangential velocity by

$$c_u = \bar{c}_u + c'_u$$

where the bar denotes the mean value and the prime denotes perturbation quantities. For a radial outlet area A, the torque required by a fluid

particle is

$$dT = \rho r c_u c_m dA ,$$

all quantities being evaluated at the impeller exit. It is assumed that c_u at the inlet is zero.

The total torque is

$$T = b\rho r \int_0^{2\pi} (\bar{c}_u + c_u')(\bar{c}_m + c_m') r \, d\theta .$$

The integral of the primed quantities must be zero by definition so that

$$T = \rho b r \left\{ 2\pi r \bar{c}_u \bar{c}_m + \int_0^{2\pi} c_u' c_m' r \, d\theta \right\} ,$$

or

$$T = \rho r \Omega \bar{c}_u + \rho b r^2 \int_0^{2\pi} c_u' c_m' \, d\theta$$

The first term is the torque, $\bar{T}$, required when the volute is not present, i.e.,

$$T = \bar{T} + T'$$

where T' is the change in torque due to the presence of the volute.

Conditions on $c_u' c_m'$: If there are an infinite number of impeller blades and if it can be assumed that they perfectly guide the flow, then the relation

$$c_m \cot \beta + c_u = u$$

follows from the exit velocity triangle and is the condition that the velocity components must satisfy. For a given $\bar{c}_u$, the average values must satisfy

$$\bar{c}_m \cot \beta + \bar{c}_u = u$$

so that

$$c_m' \cot \beta + c_u' = 0.$$

Hence, the torque relation becomes

$$T = \bar{T} - \rho b r^2 \cot \beta \int_0^{2\pi} (c_m')^2 \, d\theta .$$

It can be seen that no matter what assumptions or theories are used to compute c_m' and c_u' the torque required with volute cannot exceed that of the free impeller case.

The above deduction is not borne out by the present experiments. In fact, practically all cases show an increase in the torque required by the impeller. In arriving at the above result, there has been one main assumption, i.e., that the flow was perfectly guided by the blades. In the case of a finite number of blades in potential flow, the Kutta condition is applied at the blade tips and replaces the perfect guidance of the infinite vane case. In the current tests, the volute tongue was only about 1/16 in. away from the impeller. Thus, enormous disturbances could occur at the tips and it does not seem unreasonable that the real fluid flow cannot always adjust itself to stream smoothly off the vanes. In this event, it is possible for the term $c_m'c_u'$ to become positive and thus indicate an increase in torque required. This result also follows from the intuitive notion that the absolute flow leaving the impeller is guided or determined by the volute vanes. Thus, at high flow rates the tangential component of the absolute velocity (and corresponding torque) would be greater than in the free impeller case. If it were not for a simultaneous increase in over-all impeller losses (possibly due to oscillation of the stagnation streamline at the impeller tip) a larger average head would result. An inspection of Fig. 10 does show that the head measured 60° from the volute tongue is consistently high for high flow rates and low for the low flow rates, showing that the head there is controlled by the volute vanes.

The present analysis is admittedly speculative in part and should be subjected to further investigations. It should be clear, however, that potential flow calculation of the sort described in Ref. (4) can only be qualitative at best.

VI. CONCLUSIONS

The experimental studies of volute-impeller effects have yielded the following results:

1. At the design point of the volute its influence is least and the magnitude of the changes is small.

2. At off-design conditions large changes in pump performance occur that are due, primarily, to changes in impeller performance.

3. There are large real fluid effects in the volute flow that arise from the discharge of the rotating boundary layer into the stationary volute channel. The flow entering the volute is thus nonuniform and the resulting velocity distributions do not resemble those of a potential flow.

4. The volute passage losses are still relatively small at the volute design point (about 3 percent of the pump head) so that in spite of (3) the volute can be designed without considering the effect of friction (at least for the Reynolds numbers of these experiments).

It is also shown that at off-design conditions the flow (without friction) cannot be irrotational, so that potential flow cannot be used.

In the present experiments the maximum influence of the volute vanes has been studied. The degree of volute-impeller interference is, of course, dependent on the spacing between the volute tongue and the impeller; investigation of this variable will be undertaken in future experimental work.

REFERENCES

1. Beveridge, J. H., and Morelli, D. A., "Evaluation of a Two-dimensional Centrifugal Pump Impeller," Preprint No. 50-A-147, ASME, 1950.

2. Morelli, D. A., "Pressure Distributions on the Vanes of a Radial Flow Impeller," Trans., Heat Transfer and Fluid Mechanics Institute, 1950, p. 73. Stanford Univ. Press, Stanford, Calif., 1950.

3. Acosta, A. J., and Bowerman, R. D., "An Experimental Study of Centrifugal Pump Impellers," Calif. Institute of Technology, Hydrodynamics Laboratory Report No. E-19.8, in press.

4. Straszacker, R., "Die Ermittlung der Stromungsverhaltnisse in Spiralgehausen," Ing. Archiv, VI-3-1935, pp. 157-182.

APPENDIX I

Notation

A_2 outlet area of impeller

b impeller passage height

c absolute fluid velocity

c_m absolute meridional component of fluid velocity

c_u absolute tangential component of fluid velocity

C static head coefficient = $H_s\, g/u_2^2$

g gravitational constant

H_T total head (referenced to total head at impeller inlet)

H_S static head (referenced to total head at impeller inlet)

Q flow rate

r radius from impeller axis

r_v radial coordinate of volute vane

T torque

u impeller tangential velocity = ωr

β impeller vane angle

β_v volute vane angle

η efficiency = $\frac{\phi\psi}{\tau}$

θ angular coordinate of volute vane; absolute angular coordinate

ρ fluid density

τ torque coefficient = $\frac{T}{\rho A_2 u_2^2 r_2}$

ϕ flow rate coefficient = $c_{m2}/u_2 = Q/A_2 u_2$

ϕ_e impeller design flow rate coefficient

ψ total head coefficient = $H_T\, g/u_2^2$

ω angular velocity of impeller

Notation (cont'd)

c/u_2	dimensionless absolute fluid velocity = $\sqrt{2(\psi_v - C_v)}$

Subscripts

1	impeller inlet (β_1)
2	impeller outlet (β_2, r_2, u_2, A_2, c_{m2})
i	impeller only (ψ_i, η_i)
p	"whole pump" (impeller with volute) (ψ_p, η_p)
x	design quantity (ψ_x, ϕ_x, η_x)
v	refers to volute quantity (ψ_v, C_v)

APPENDIX II

Method of Calculating Volute Vane Shapes

For uniform discharge from the impeller,

$$Q_\theta = \frac{\theta}{2\pi} Q$$

where Q_θ = discharge through annular section, θ. For constant angular momentum, the velocity in the tangential direction must be:

$$c_{u_r} = c_{u2} \frac{r_2}{r} .$$

The flow rate at an angle θ from the leading edge of the volute is:

$$Q_\theta = Q\frac{\theta}{2\pi} = b \int_{r_2}^{r_v} c_{u_r} \, dr = b \int_{r_2}^{r_v} \frac{c_{u2}}{r} r_2 \, dr .$$

Then,

$$Q \frac{\theta}{2\pi} = b \, r_2 \, c_{u2} \, \ell n \, (\frac{r_v}{r_2})$$

and solving for r_v

$$r_v = r_2 \, e^{\frac{Q\theta}{2\pi \, b \, r_2 \, c_{u2}}} .$$

This equation is the familiar logarithmic spiral. The final form of the equation is obtained as follows:

$$Q = c_{m2} A_2 = c_{m2} \, 2\pi \, r_2 \, b$$

so,

$$r_v = r_2 \, e^{\frac{c_{m2}}{c_{u2}} \theta} .$$

Furthermore, the volutes were designed to match the actual outlet flow angle of the free impeller by relating the measured head of the free impeller to the tangential component of the absolute velocity:

$$H = \frac{\eta \, u_2 \, c_{u2}}{g}$$

where η is the measured efficiency. With the additional consideration

of the dimensionless coefficients $\psi = \frac{Hg}{u_2^2}$ and $\phi = \frac{c_{m2}}{u_2}$

then $$\frac{c_{m2}}{c_{u2}} = \frac{\phi\eta}{\psi}$$

and

$$r_v = r_2 \, e^{\frac{\phi\eta}{\psi}\theta}$$

APPENDIX III

Derivation of the Theoretical Head Equation

(Bernoulli's Equation in a Rotating Co-ordinate System)

Given, two co-ordinate systems with a common origin where one system is fixed and the other rotates with constant angular velocity, ω. A particle (element of fluid) at a point in space with position vector $\bar{r}$ can be shown to have an absolute acceleration:

$$\bar{a} = \frac{d^2\bar{r}}{dt^2} = \frac{\delta^2\bar{r}}{\delta t^2} + 2\bar{\omega} \times \frac{\delta\bar{r}}{\delta t^2} + \bar{\omega} \times \bar{\omega} \times \bar{r} ,$$

where $\delta/\delta t$ means differentiation in the rotating or relative system.

Let $\frac{\delta\bar{r}}{\delta t} = \bar{w}$ = relative velocity vector,

then $\frac{\delta^2\bar{r}}{\delta t^2} = \frac{\delta\bar{w}}{\delta t} = \frac{\partial\bar{w}}{\partial t} + \bar{w} \cdot \nabla\bar{w}$.

Substituting in the equation of motion,

$$\bar{a} = -\frac{1}{\rho}\nabla p + \text{body forces} = \frac{\partial\bar{w}}{\partial t} + \bar{w} \cdot \nabla\bar{w} + 2\bar{\omega} \times \bar{w} + \bar{\omega} \times \bar{\omega} \times \bar{r} .$$

The body forces are neglected.

Substituting for vector identities gives:

$$\frac{\partial\bar{w}}{\partial t} + \nabla\left(\frac{w^2}{2}\right) - \bar{w} \times \nabla \times \bar{w} + 2\bar{\omega} \times \bar{w} + (\bar{\omega} \cdot \bar{r})\,\bar{\omega} - \omega^2\bar{r} = -\frac{\nabla p}{\rho} .$$

Assuming a two-dimensional flow and multiplying through by an element of streamline, $d\bar{s} = d\bar{r} = \bar{w}\,dt$, the vector quantities perpendicular to $\bar{w}$ drop out leaving:

$$\frac{\partial\bar{w}}{\partial t} \cdot d\bar{s} + \nabla\left(\frac{w^2}{2} + \frac{p}{\rho}\right) \cdot d\bar{s} - \omega^2\bar{r} \cdot d\bar{r} = 0$$

or

$$d\left(\frac{w^2}{2} - \frac{r^2\omega^2}{2} + \frac{p}{\rho}\right) + \frac{\partial\bar{w}}{\partial t} \cdot d\bar{s} = 0.$$

Integrating along a streamline with time held constant from (1) corresponding to the impeller inlet, to (2) corresponding to the impeller exit, yields:

$$(1) \ldots \quad \frac{p_2}{\rho} + \frac{1}{2}(w_2^2 - r_2^2\omega^2) - \frac{p_1}{\rho} - \frac{1}{2}(w_1^2 - r_1^2\omega^2) + \int_{(1)}^{(2)(S)} \frac{\partial \bar{w}}{\partial t} \cdot d\bar{s} = 0.$$

When $\frac{\partial \bar{w}}{\partial t} = 0$ this reduces to the usual expression for Bernoulli's equation in rotating co-ordinates.

It is possible to evaluate the term $\int_{(1)}^{(2)(S)} \frac{\partial \bar{w}}{\partial t} \cdot d\bar{s}$ as follows:

Considering the velocity triangle for an impeller and assuming an infinite number of vanes.

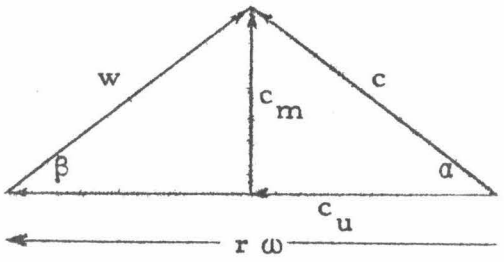

$( )_2$ impeller exit

$( )_1$ impeller inlet

then $w = \frac{c_m}{\sin\beta}$ $\quad ds = \frac{dr}{\sin\beta}$

and for continuity $c_m r = c_{m2} r_2$; $\quad wr = w_2 r_2$;

so, $\frac{\partial c_m}{\partial t} = \frac{r_2}{r} \frac{\partial c_{m2}}{\partial t} = \frac{r_2}{r} \frac{dc_{m2}}{d\theta} \frac{d\theta}{dt}$.

With $\frac{d\theta}{dt} = \omega$,

then $\frac{\partial w}{\partial t} = \frac{r_2}{r} \frac{\omega}{\sin\beta} \frac{dc_{m2}}{d\theta}$.

Now,

$$\int_{(1)}^{(2)(S)} \frac{\partial \bar{w}}{\partial t} \cdot d\bar{s} = \frac{r_2\omega}{\sin^2\beta_2} \frac{dc_{m2}}{d\theta} \int_{r_1}^{r_2} \frac{dr}{r}$$

$$= \frac{r_2\omega}{\sin^2\beta_2} \frac{dc_{m2}}{d\theta} \ln\left(\frac{r_2}{r_1}\right).$$

Combining Eq. (1) with the head equation,

$$H = h_2 - h_1 = \frac{p_2 - p_1}{\rho g} + \frac{c_2^2 - c_1^2}{2g}$$

gives:

$$H = \frac{c_2^2 + r_2^2\omega^2 - w_2^2}{2g} - \frac{c_1^2 + r_1^2\omega^2 - w_1^2}{2g} - \frac{r_2\,\omega}{g \sin^2\beta_2} \frac{dc_{m2}}{d\theta} \ln\left(\frac{r_2}{r_1}\right),$$

where $\omega r = u$.

Referring to the velocity triangle and employing the cosine law, the head equation reduces to:

$$H = \frac{u_2 c_2 \cos\alpha_2}{g} - \frac{u_1 c_1 \cos\alpha_1}{g} - \frac{u_2}{g \sin^2\beta_2} \frac{dc_{m2}}{d\theta} \ln\left(\frac{r_2}{r_1}\right).$$

At the off design flow rates of the volute, c_{m2} cannot be constant around the impeller periphery, i.e., $dc_{m2}/d\theta \neq 0$. Therefore, the Bernoulli constant varies around the exit (although the Bernoulli constant is presumed uniform at the impeller inlet) and so the flow cannot be irrotational.

APPENDIX IV

Table of Constants

Volute Equation: $r_v = r_2 e^{\frac{\phi\eta}{\psi}\theta}$

Impeller Vane Angles: $\beta_1 = 20^\circ$, $\beta_2 = 23.5^\circ$

$r_2 = 5.15"$ $\quad b = 1.2"$ $\quad \phi_e = 0.1170$

Percent Free Impeller Design Point	ϕ_x*	ψ_x*	η_x*	$\frac{\phi_x \eta_x}{\psi_x}$	β_v	Volute Designation
75%	0.0878	0.568	0.920	0.143	8.1°	75% Volute
100%	0.1170	0.475	0.925	0.2278	12.8°	100% Volute
120%	0.1404	0.405	0.915	0.3163	17.6°	120% Volute

For N = 150 RPM

$u_2 = 6.74$ ft/sec

ΔH (ft) = 1.411 (ψ or C)

Q (cfs) = 1.739 ϕ

T (ft lb) = 9.747 τ

Reynolds No. = $\frac{\omega r_2^2}{\nu} = 2.4 \times 10^5$

Running Clearances

Radial; .005" – .008"

Inlet seal; .004"

Volute tongue;

.015" from impeller shrouds

.020" from impeller vanes

* Measured free impeller characteristics, ψ measured 1/16" from impeller exit.

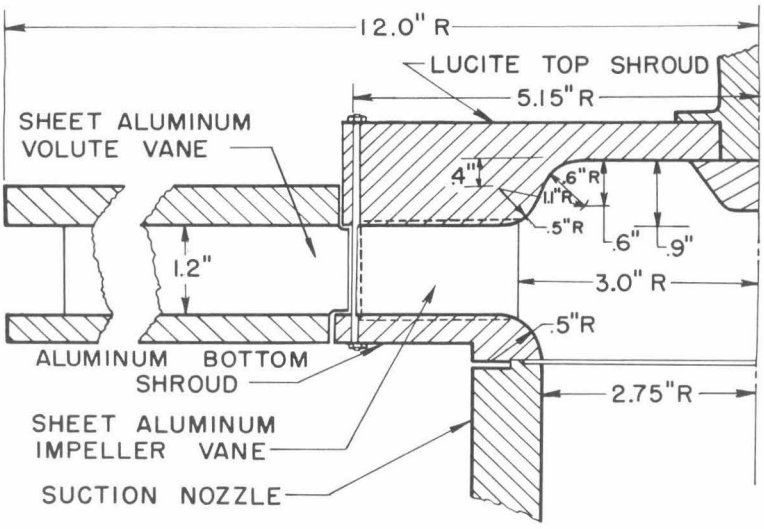

Fig. 1a - Axial cross section of test pump.

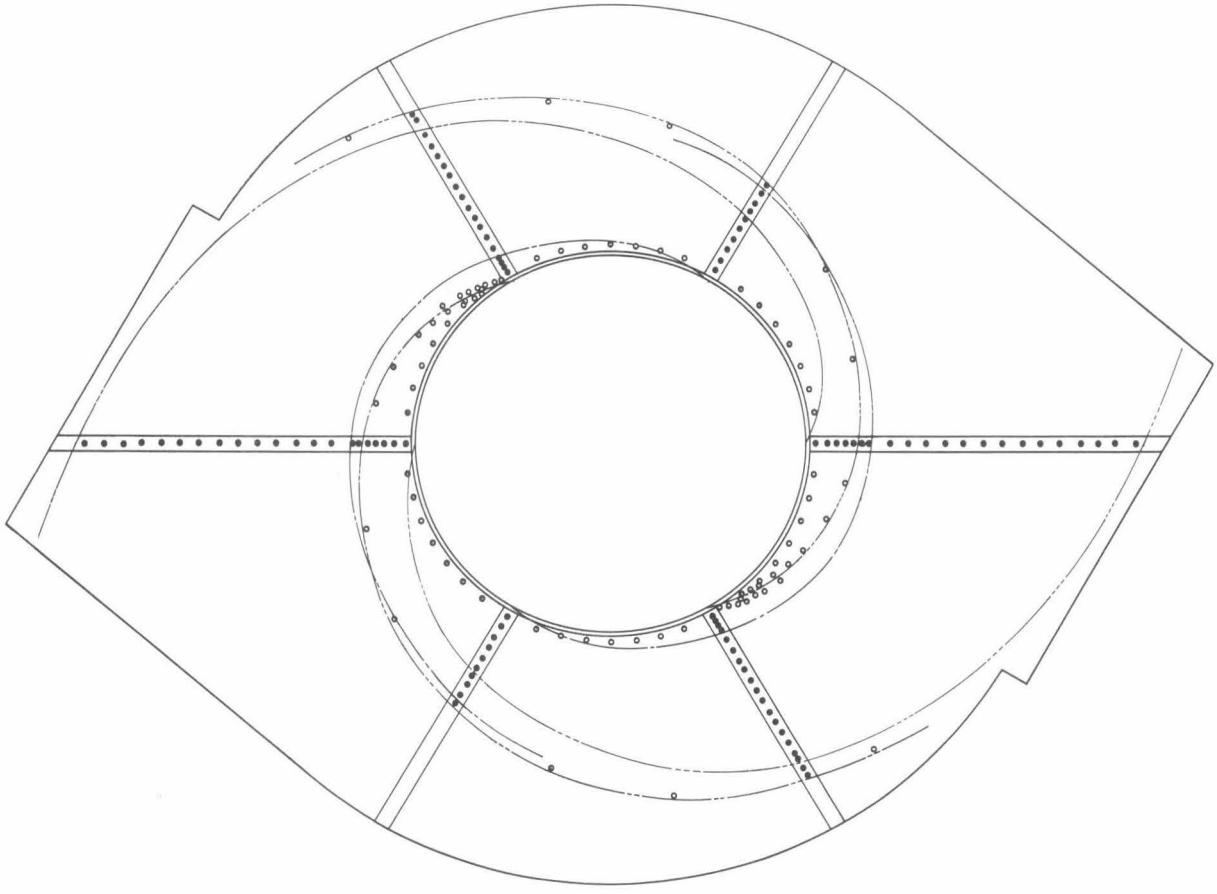

Fig. 1b - Layout of volute vanes in diffuser shrouds. Position of piezometer taps shown as follows:-

- o indicates static tap;
- ● indicates static tap and total head probe.

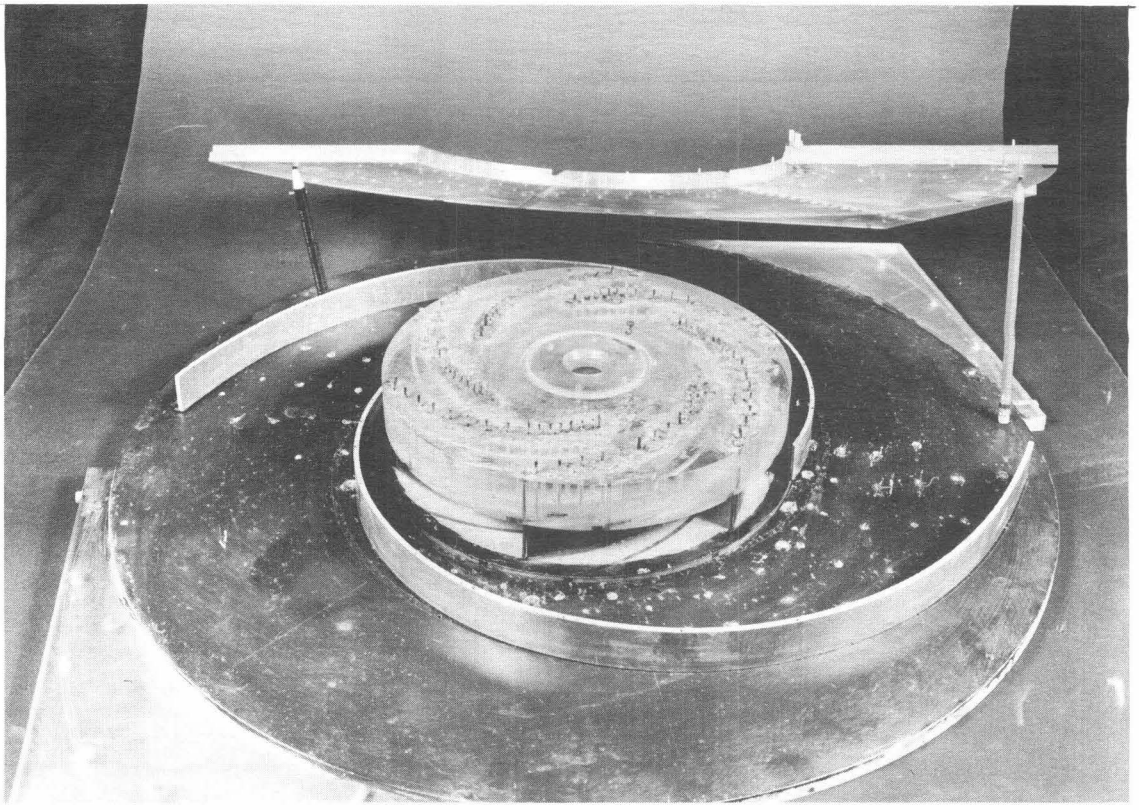

Fig. 2a - Assembly view of pump components.

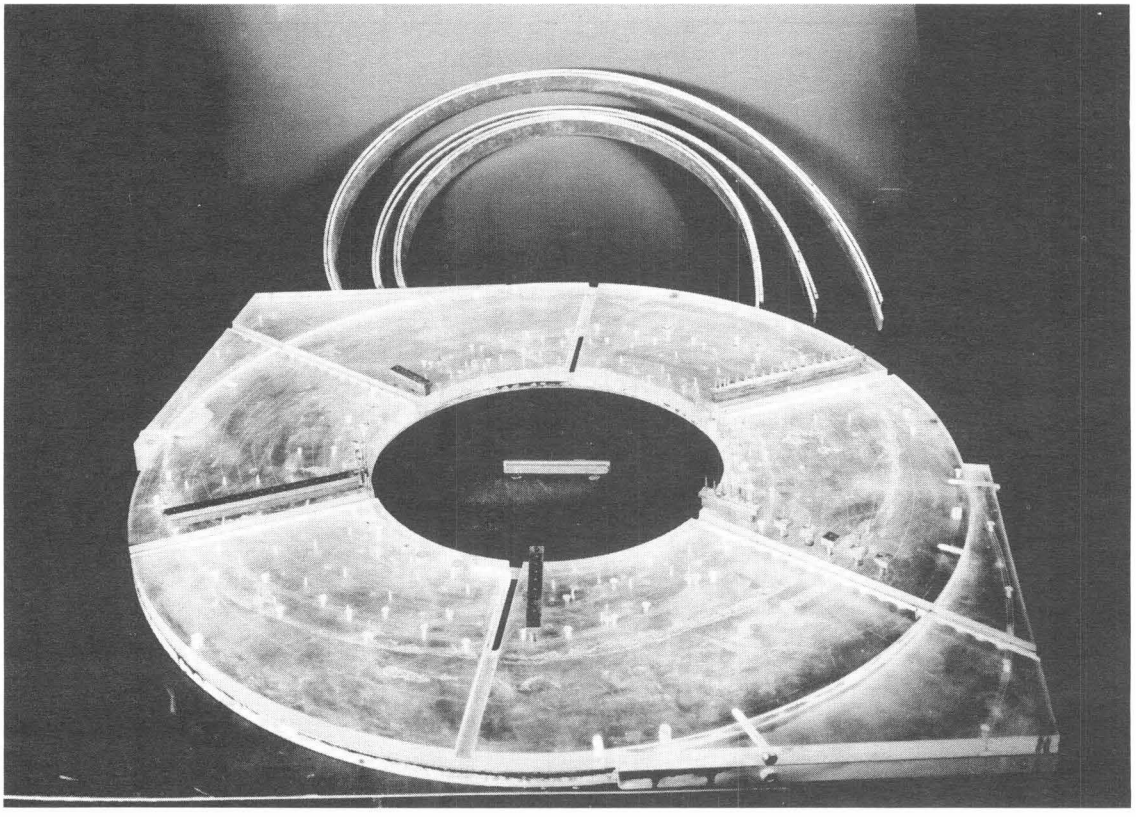

Fig. 2b - Top shroud with probe sections beside receptive slots. The three sets of volute vanes are above.

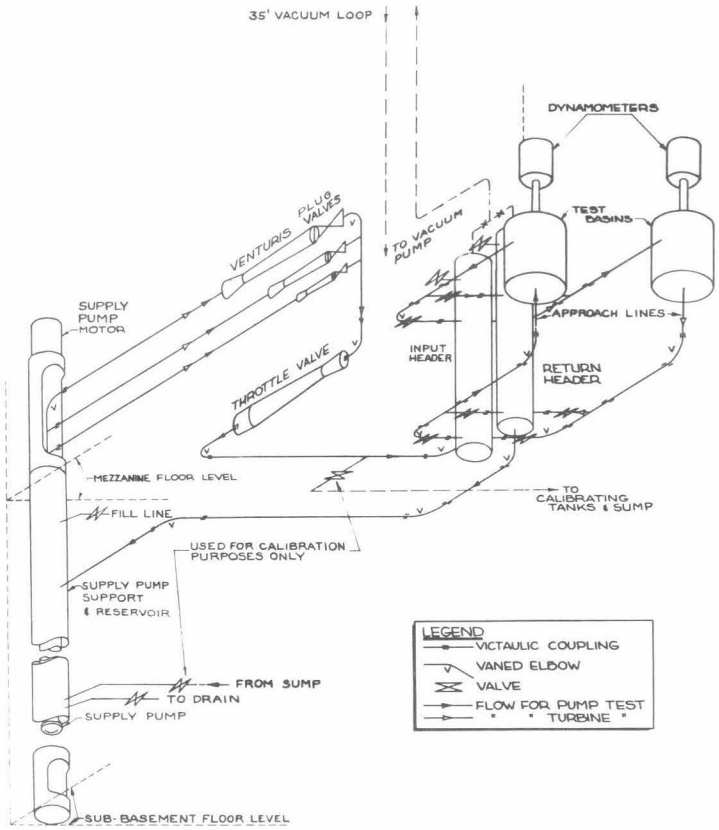

Fig. 3 - Schematic diagram of test circuit.

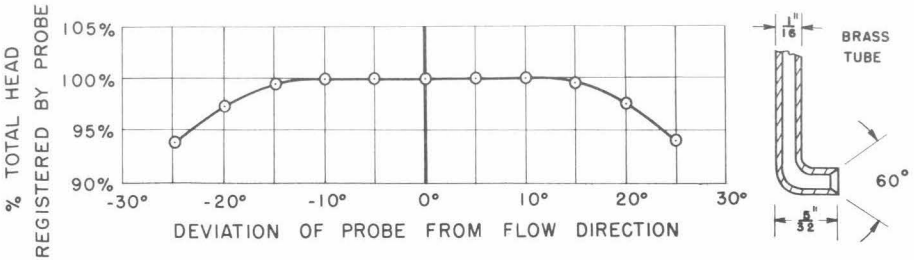

Fig. 5 - Angle sensitivity of total head probes.

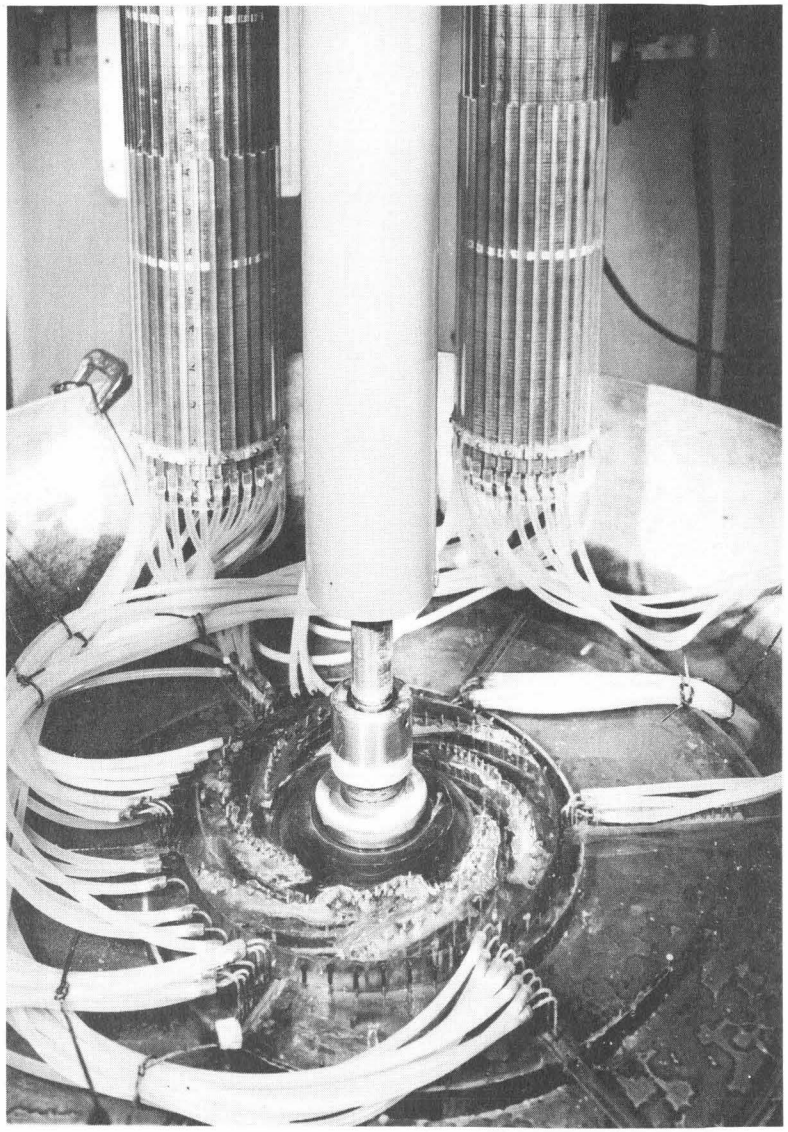

Fig. 4 - Instrumented pump in test basin.

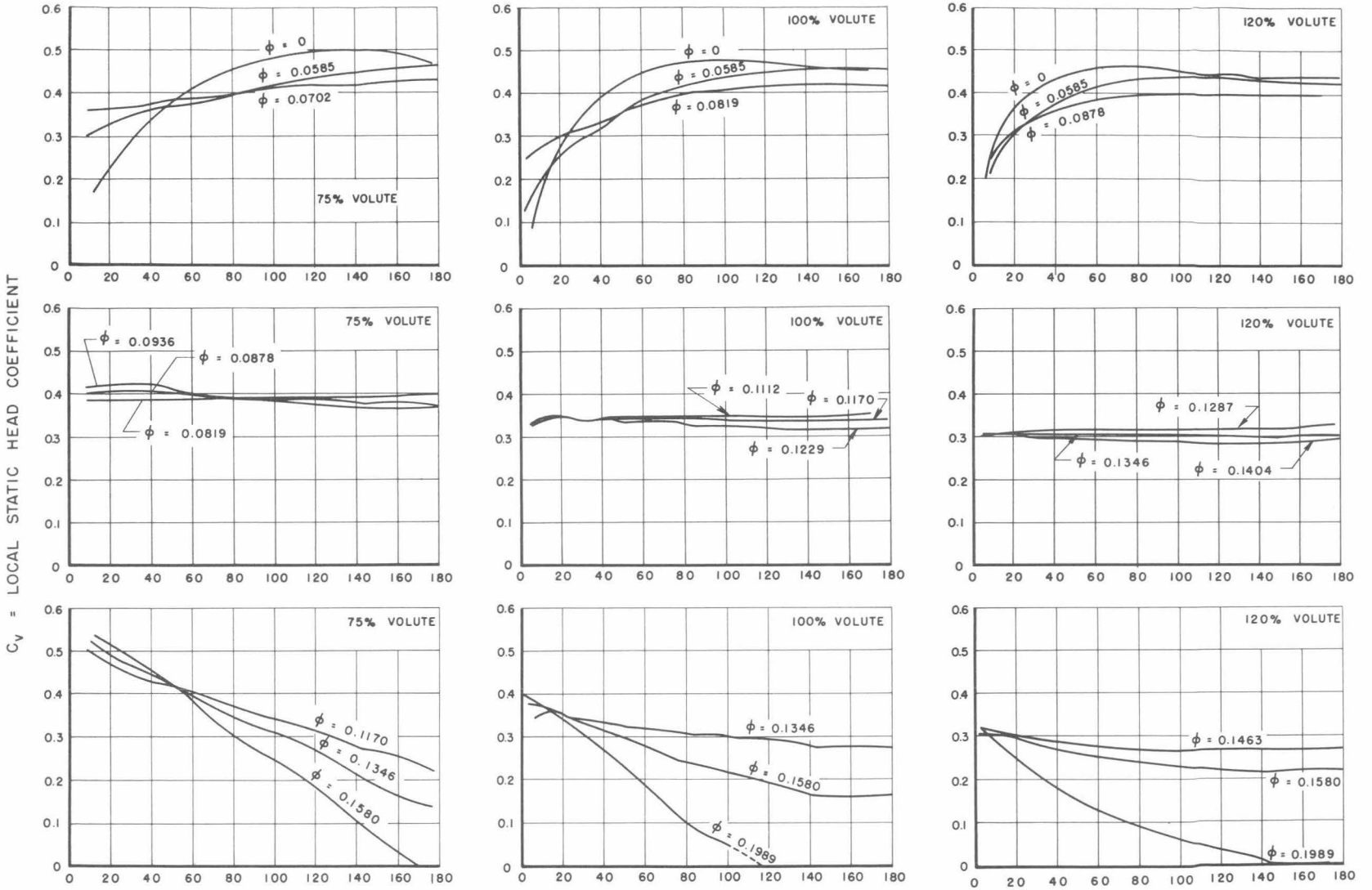

Fig. 6 - Static head coefficient around the impeller periphery for the three volute shapes at selected flow rate coefficients.

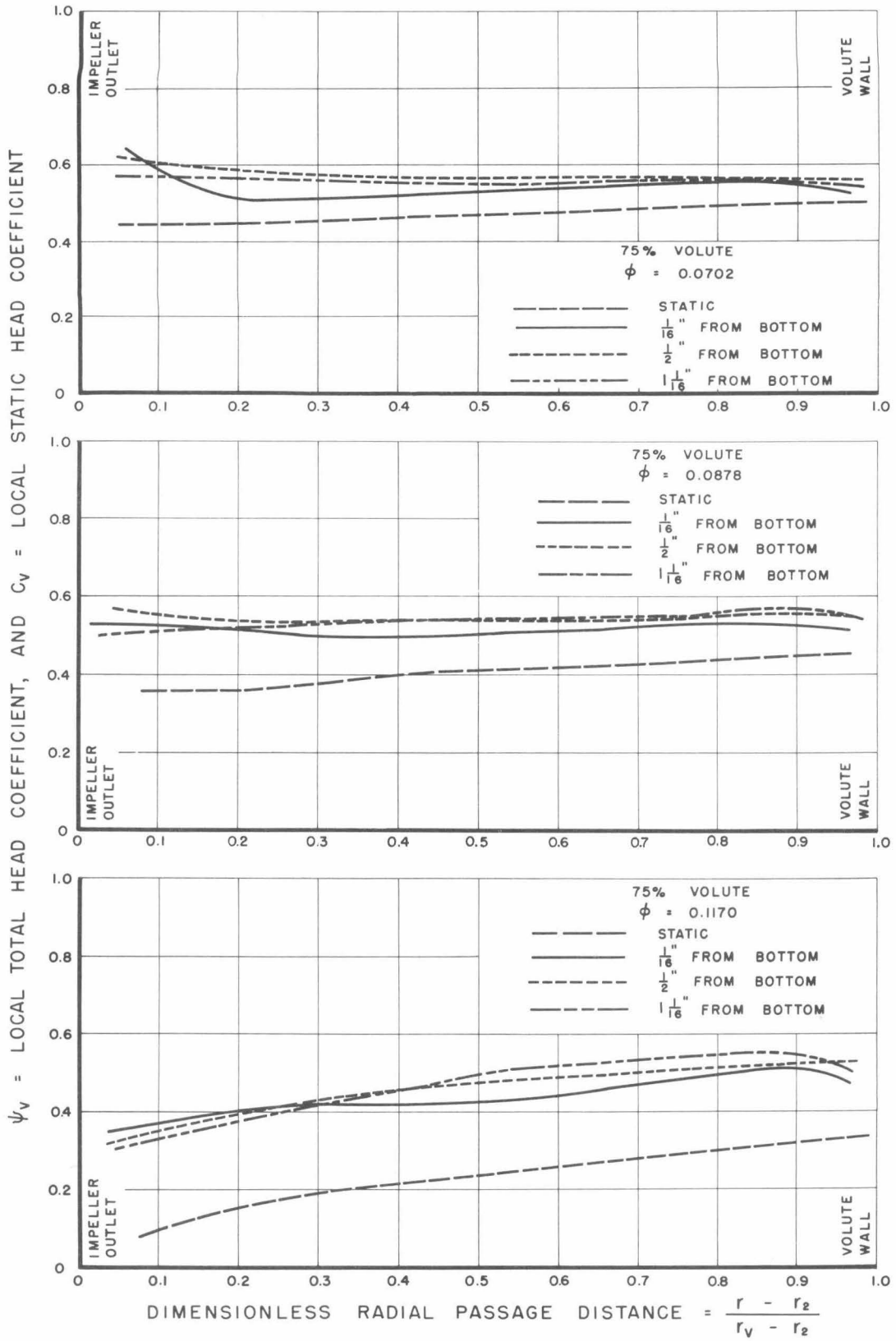

Fig. 7 - Local static head coefficient and local total head coefficients at three levels from the bottom shroud for the three volute shapes at selected flow rate coefficients.

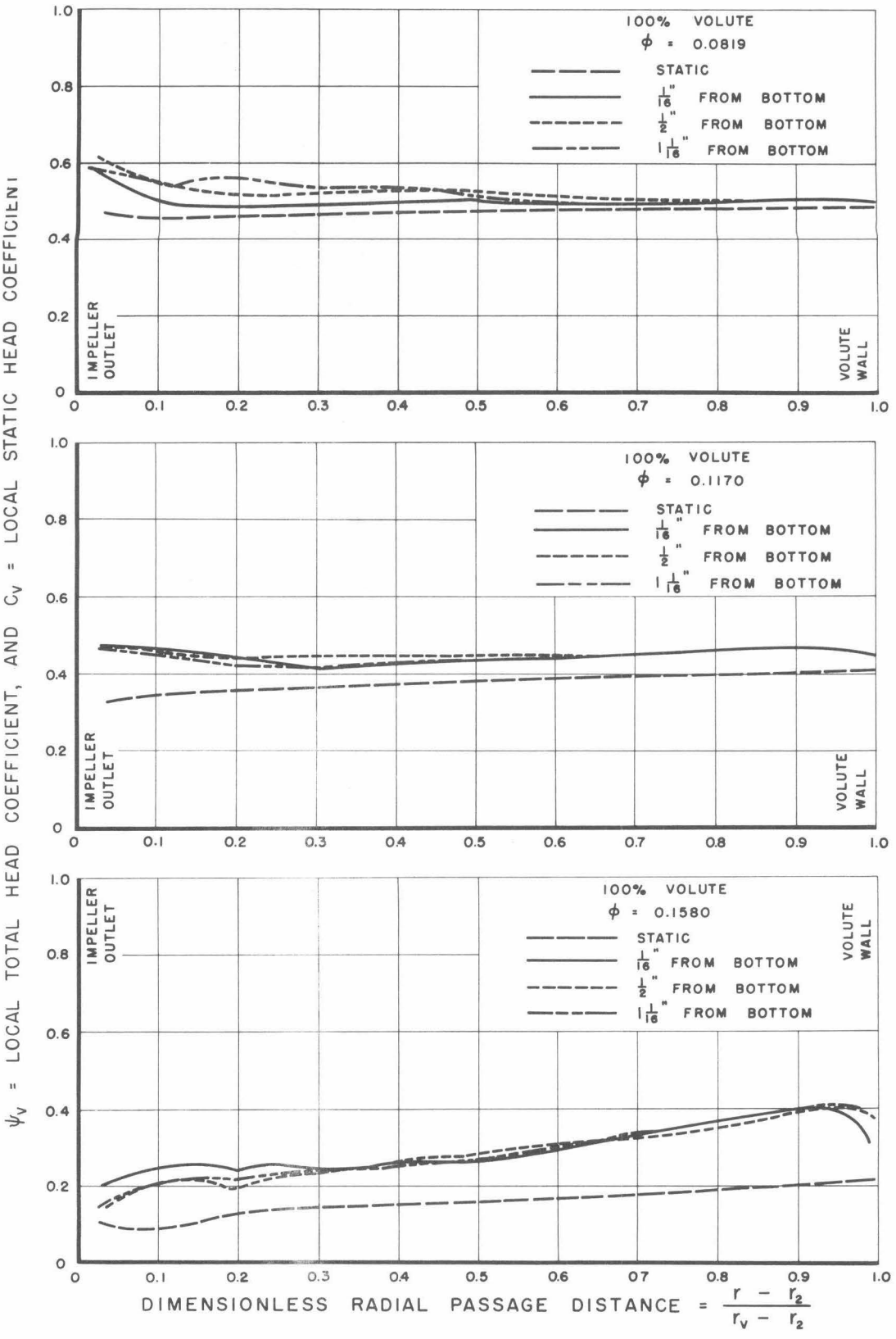

Fig. 7 (continued) - Local static head coefficient and local total head coefficients at three levels from the bottom shroud for the three volute shapes at selected flow rate coefficients.

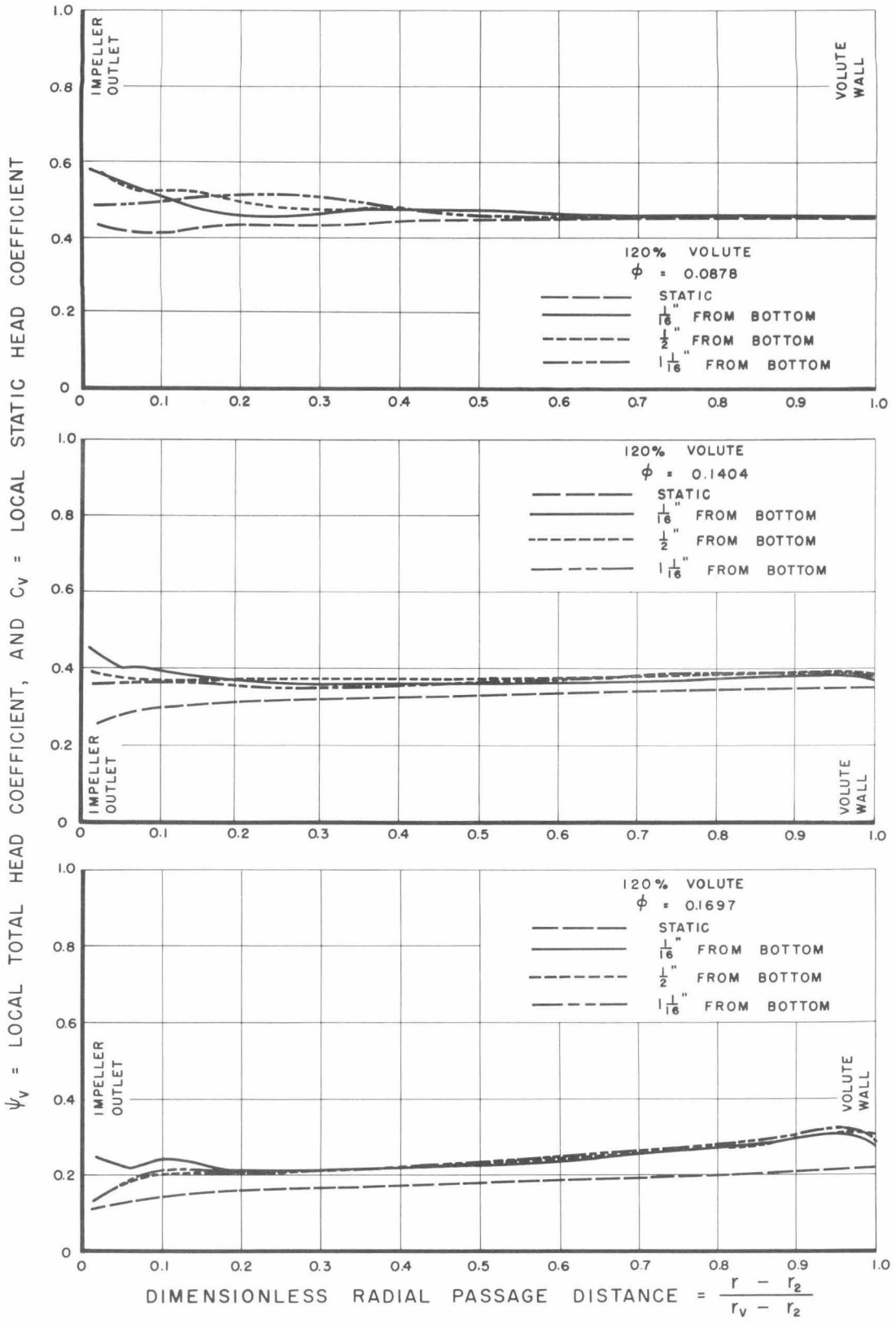

Fig. 7 (concluded) - Local static head coefficient and local total head coefficients at three levels from the bottom shroud for the three volute shapes at selected flow rate coefficients.

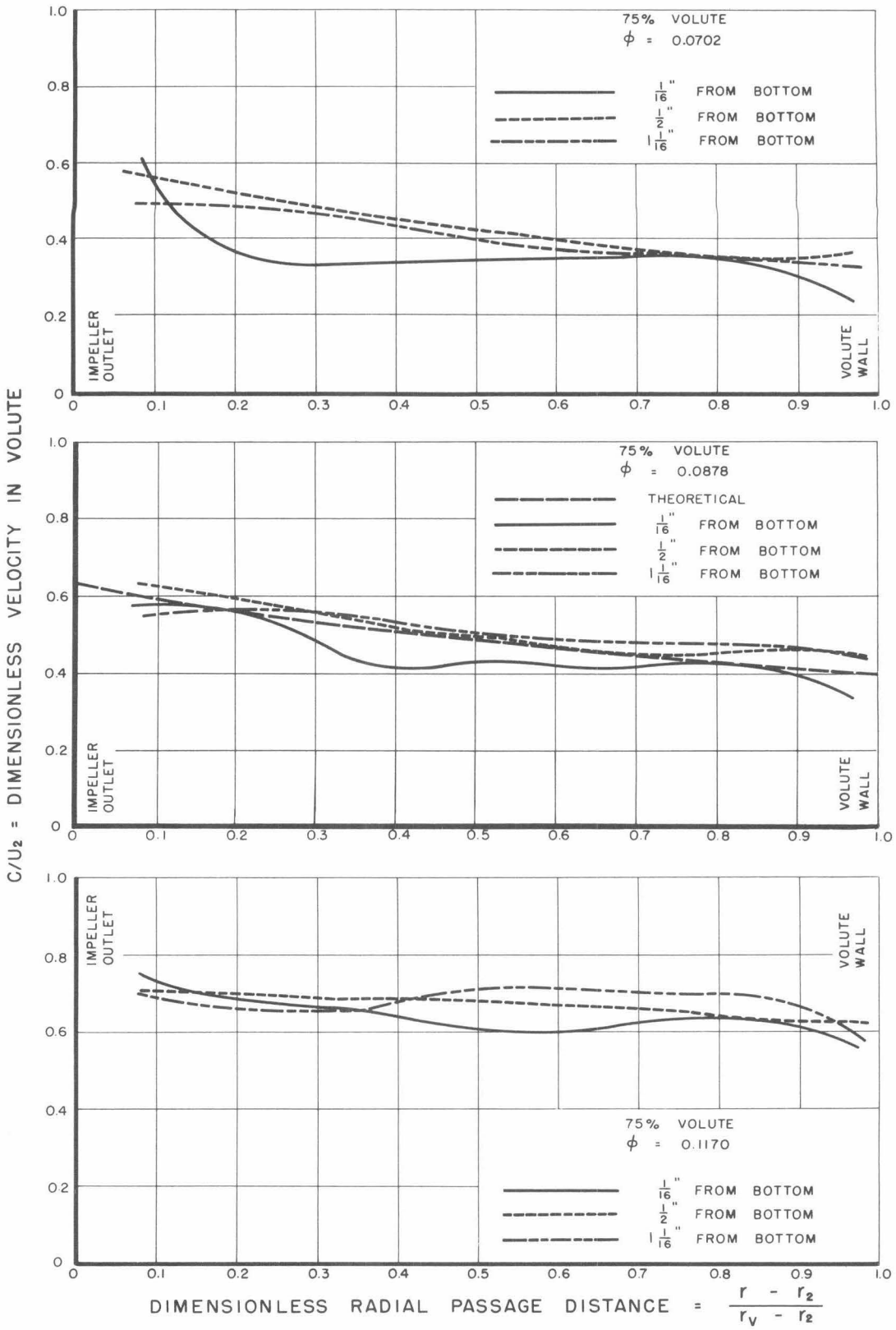

Fig. 8a - Horizontal velocity profiles at three levels from the bottom shroud at the volute exit (180^{o} from tongue) for the three volute shapes at selected flow rates.

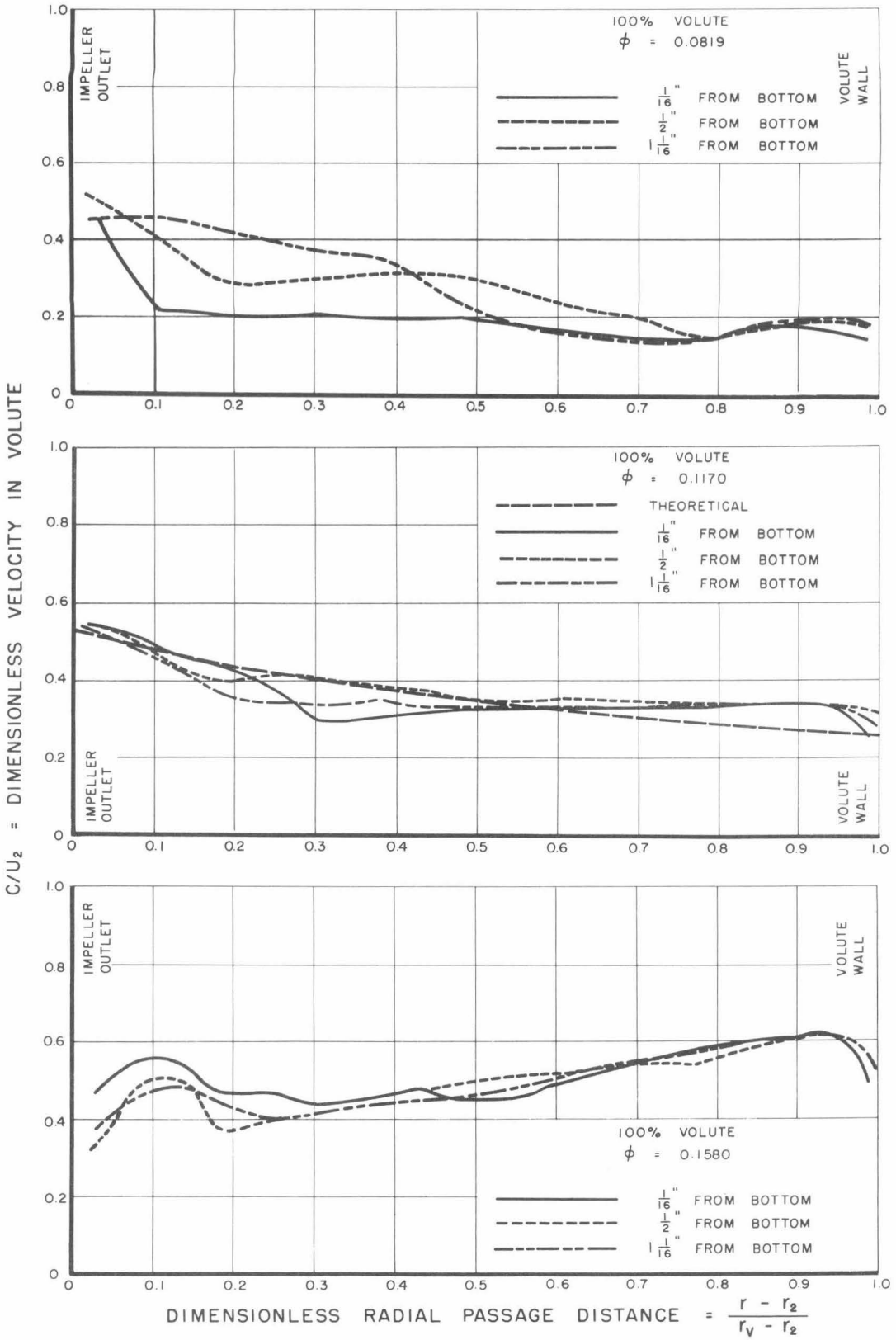

Fig. 8a (continued) - Horizontal velocity profiles at three levels from the bottom shroud at the volute exit (180° from tongue) for the three volute shapes at selected flow rates.

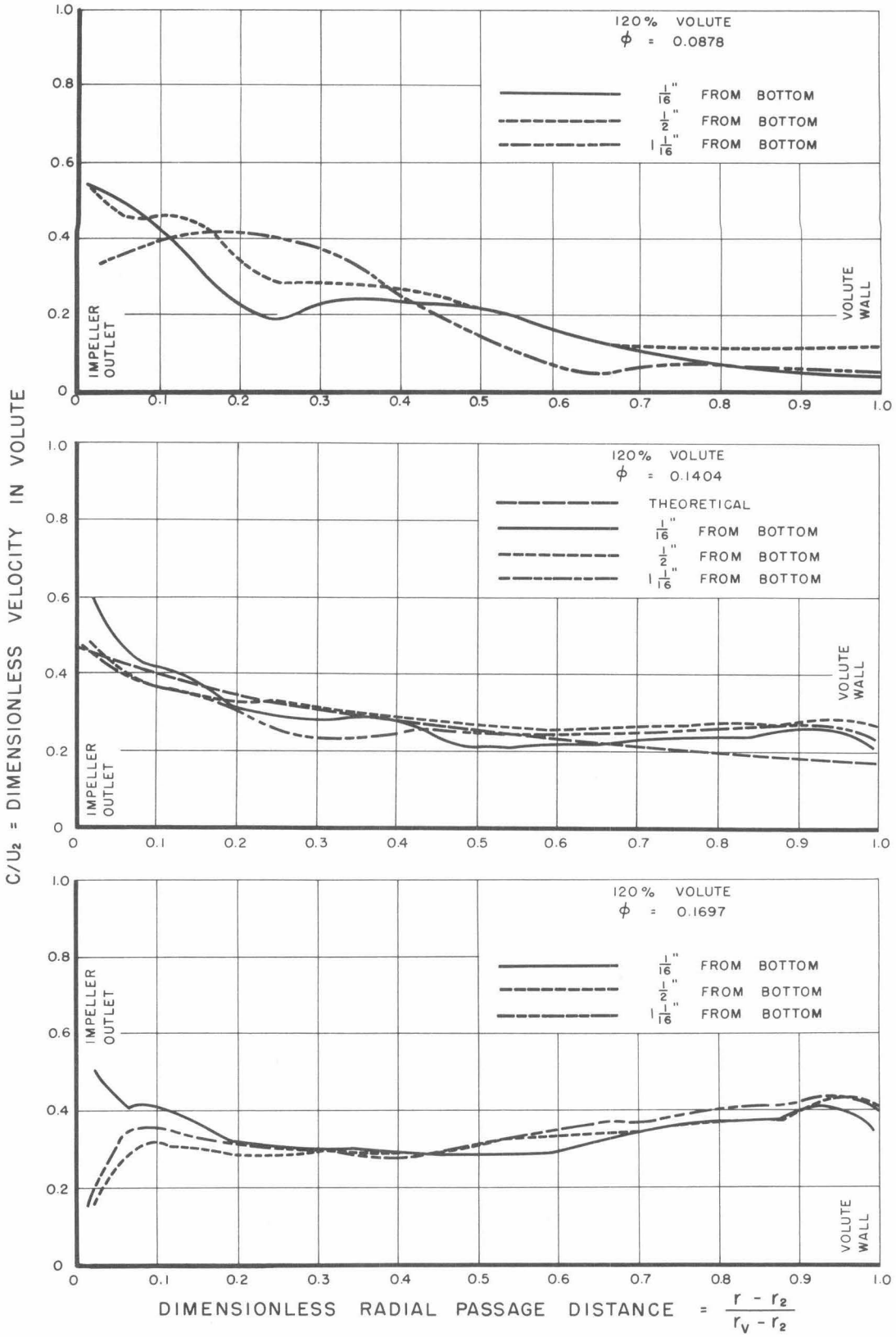

Fig. 8a (concluded) - Horizontal velocity profiles at three levels from the bottom shroud at the volute exit (180° from tongue) for the three volute shapes at selected flow rates.

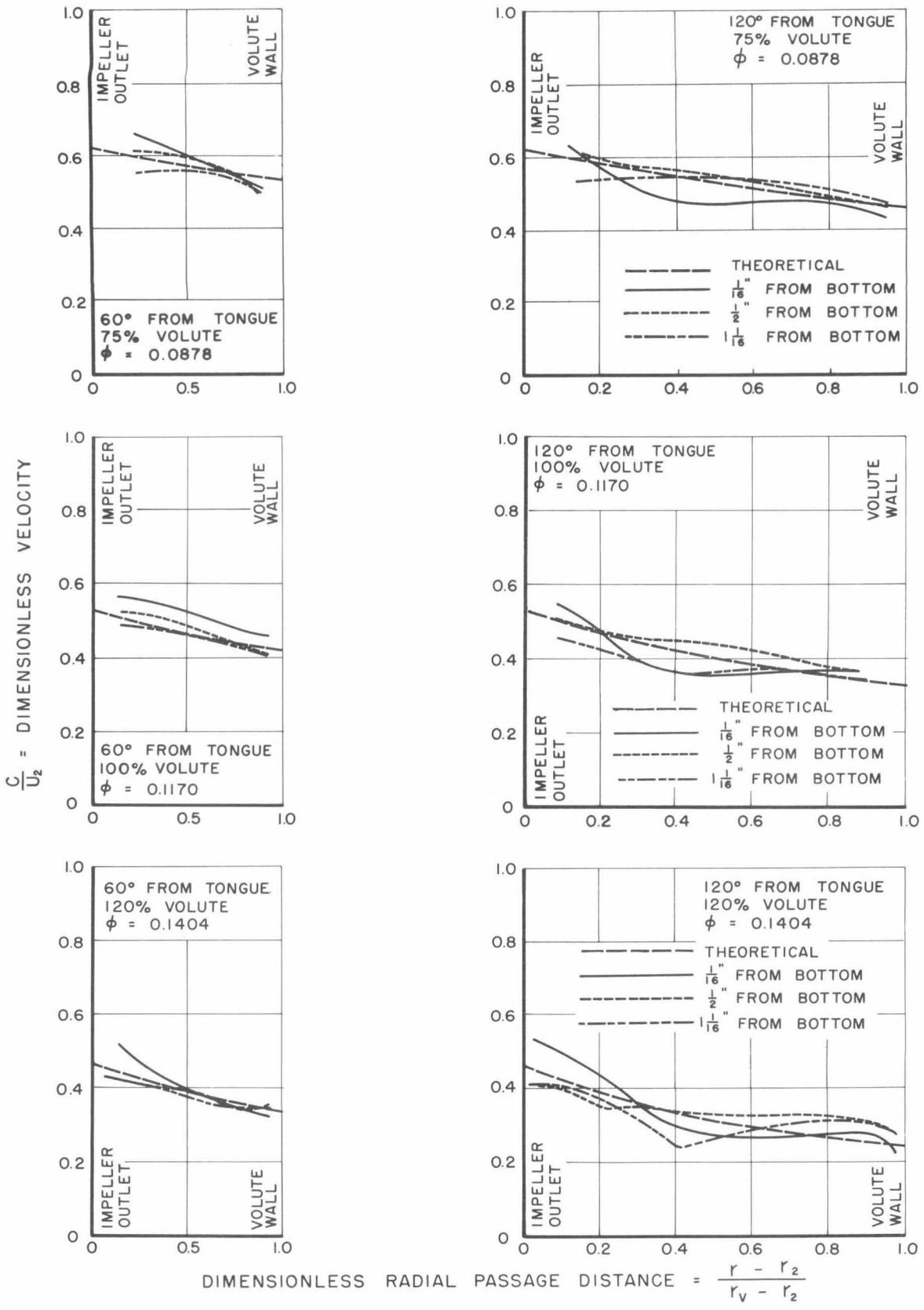

Fig. 8b - Horizontal velocity profiles at three levels from the bottom shroud at the 60° and 120° positions from the tongue for the three volute shapes at their design flow rates.

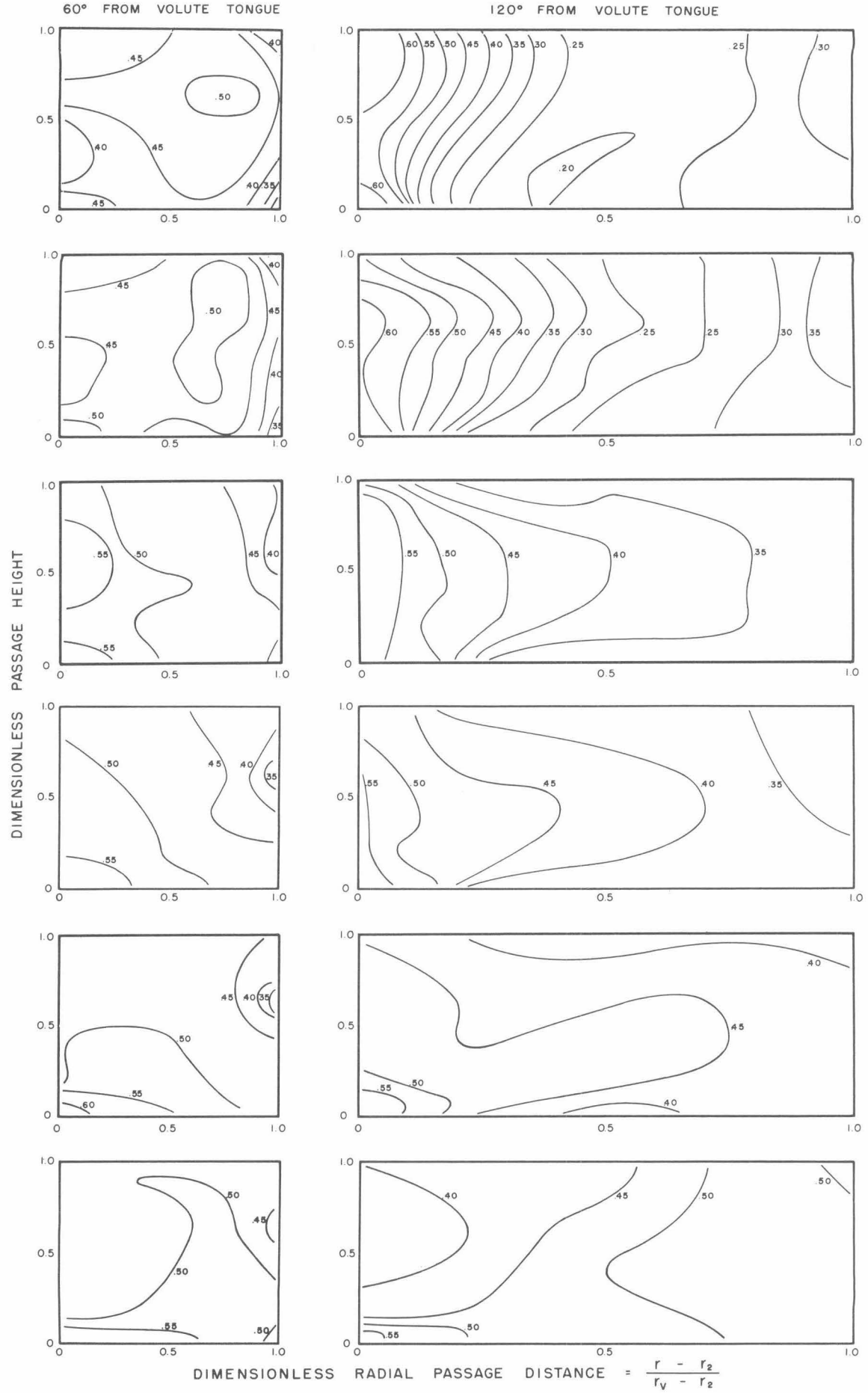

Fig. 9 - Velocity contours (lines of constant c/u_2) for the 100% volute at the

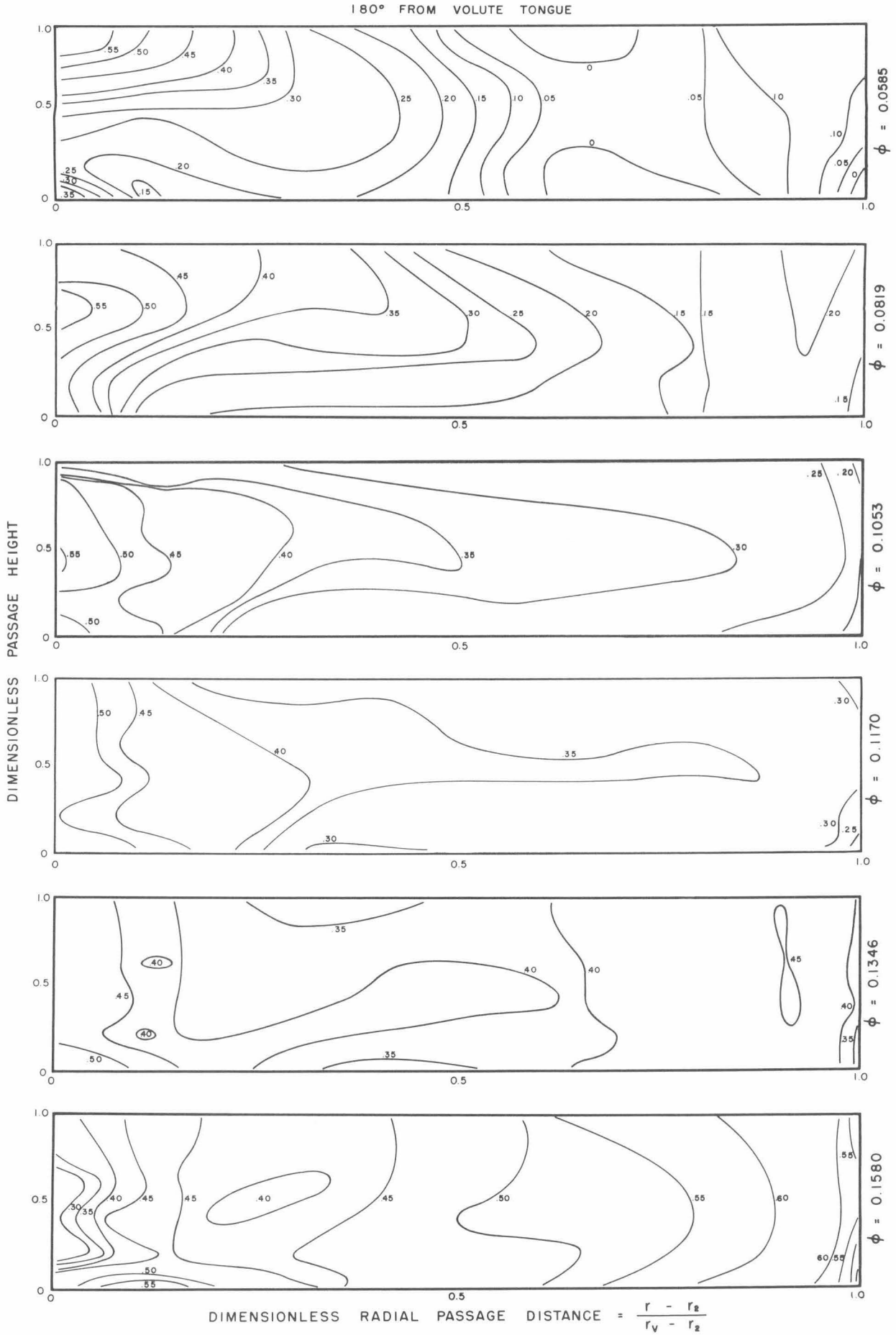

60°, 120° and 180° positions from the volute tongue at selected flow rates.

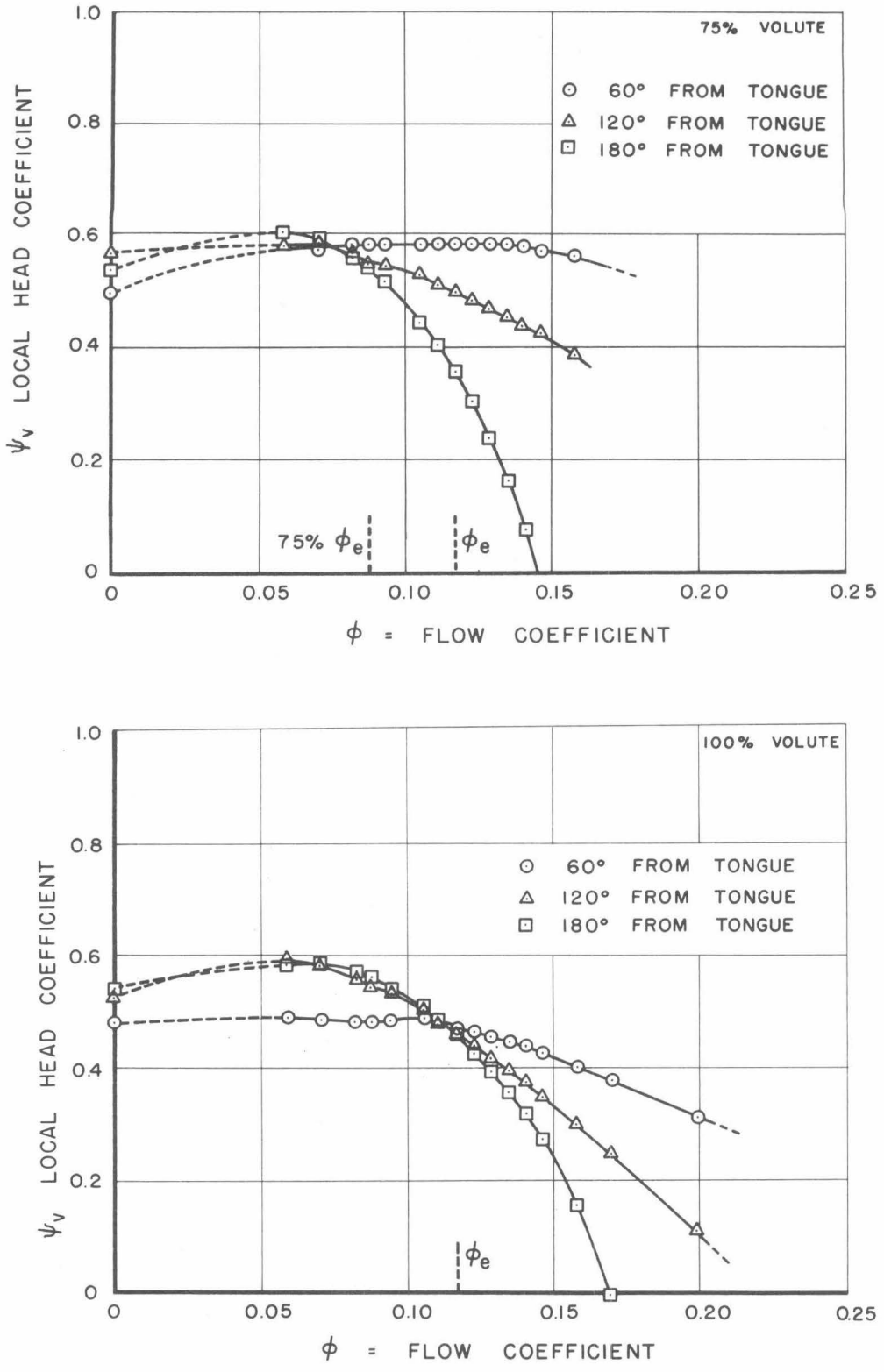

Fig. 10 - Impeller head coefficient measured at the 60°, 120°, and 180° positions from the volute tongue for the three volute shapes.

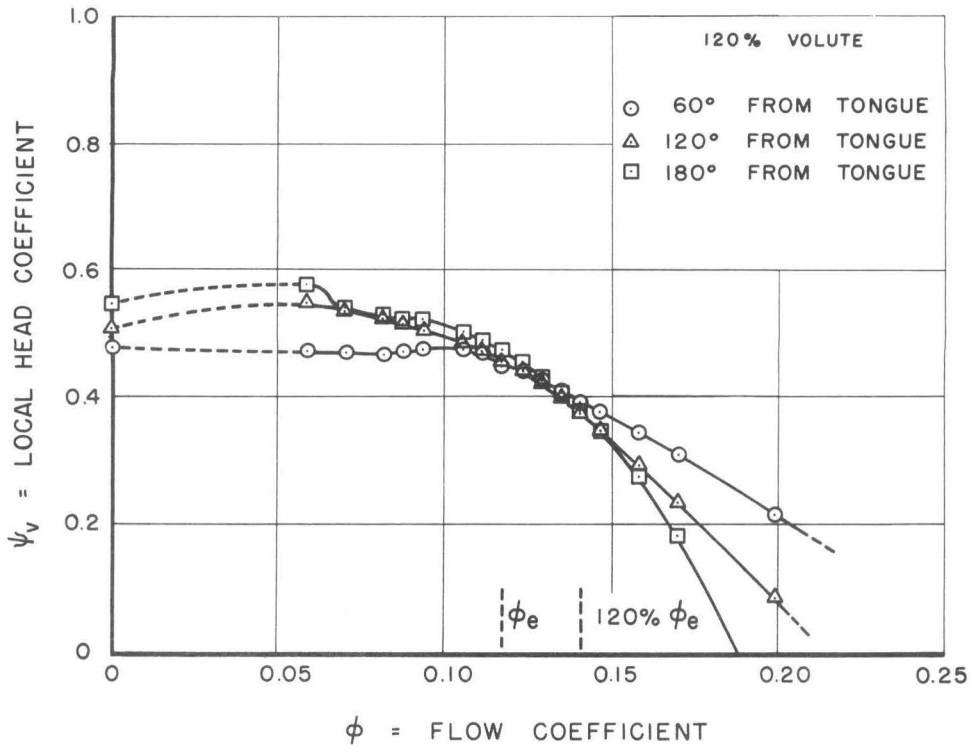

Fig. 10 (concluded) - Impeller head coefficient measured at the 60°, 120° and 180° positions from the volute tongue for the three volute shapes.

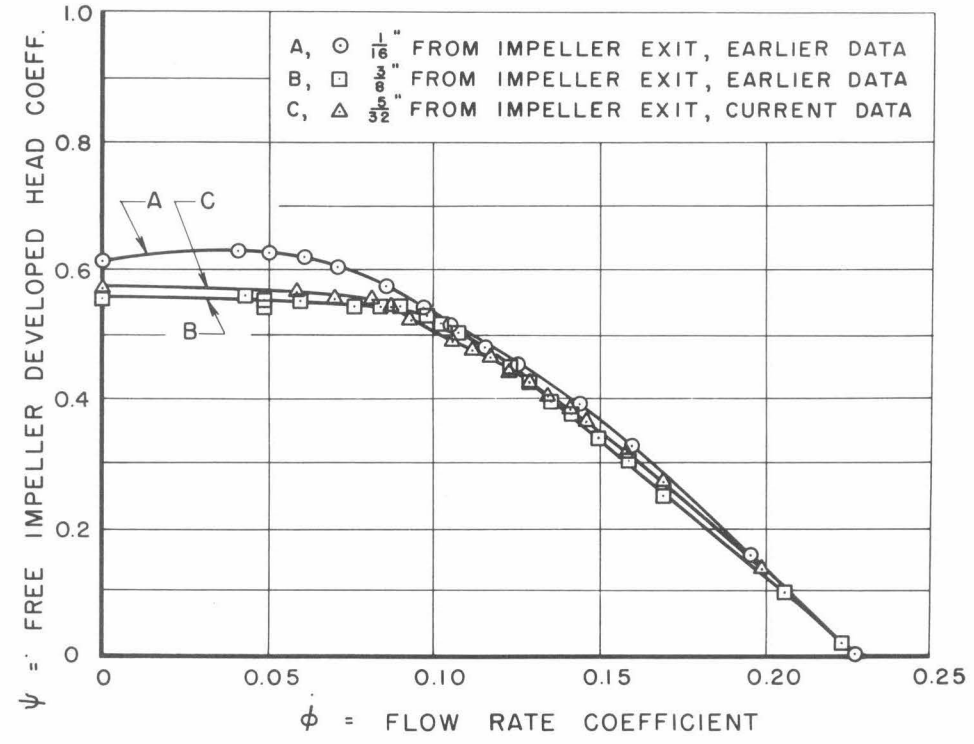

Fig. 11 - Free impeller developed head coefficient measured at three distances from the impeller exit.

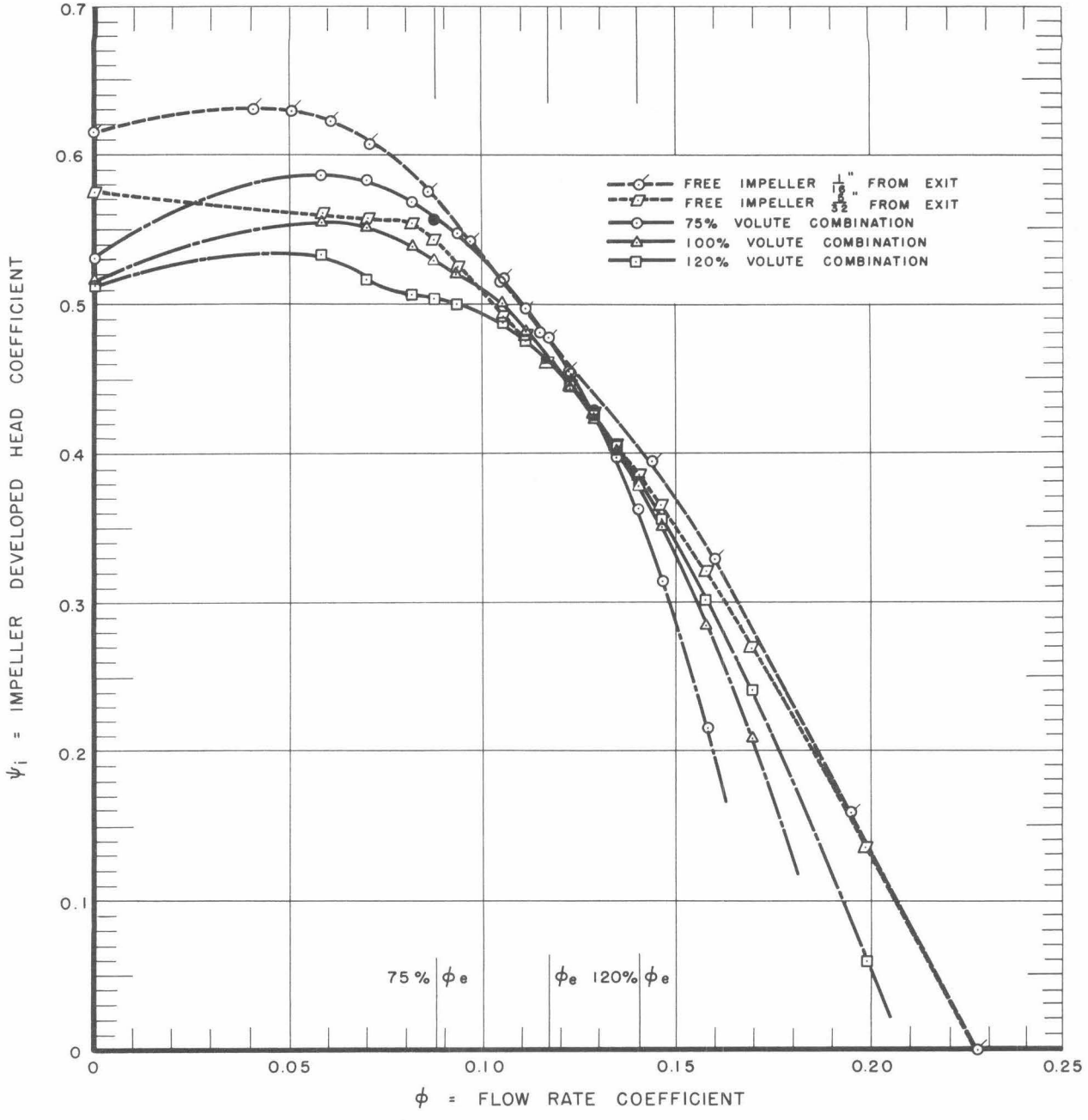

Fig. 12 - Impeller developed head coefficient for the three volute shapes and the free impeller.

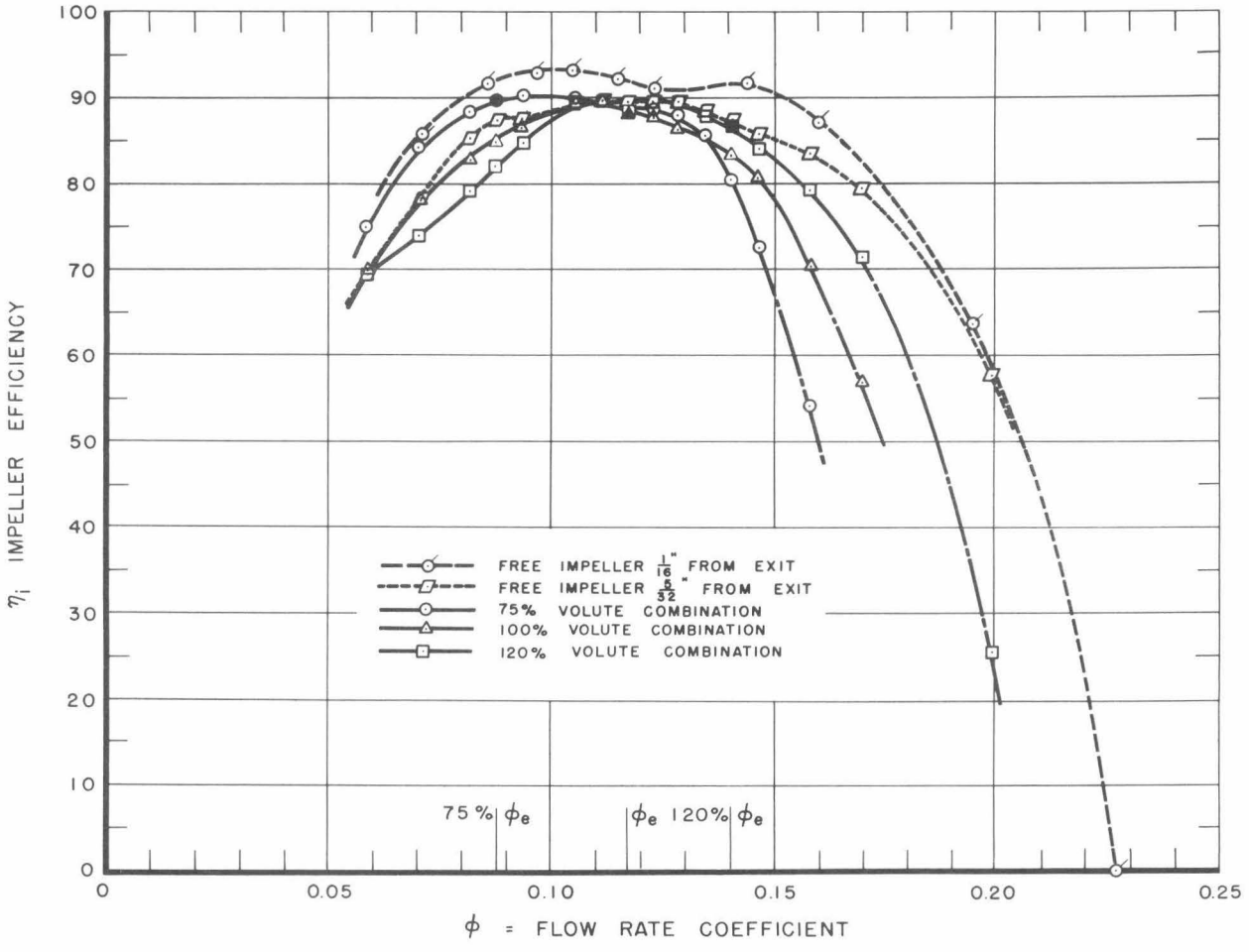

Fig. 13 - Impeller efficiency for the three volute shapes and the free impeller.

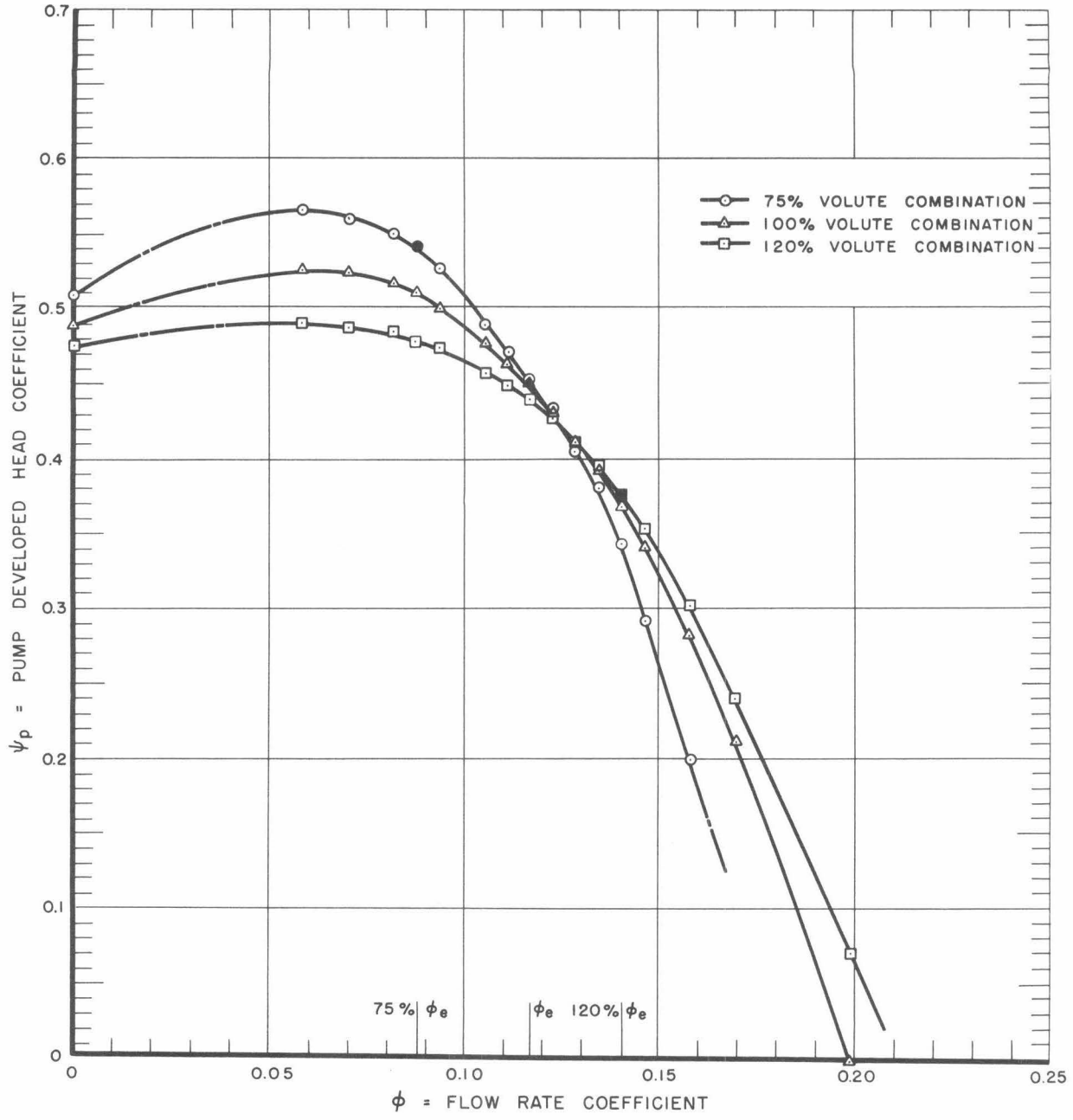

Fig. 14 - Pump developed head coefficient for the three impeller-volute combinations.

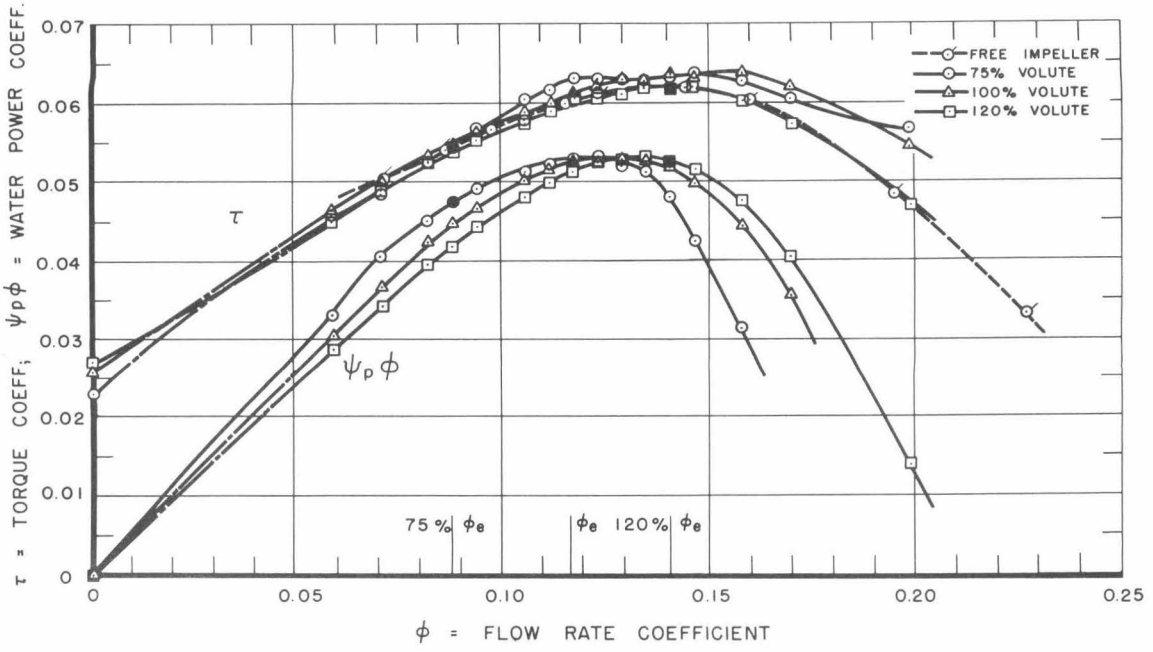

Fig. 15 - Torque coefficient and pump water power coefficient for the three volute shapes.

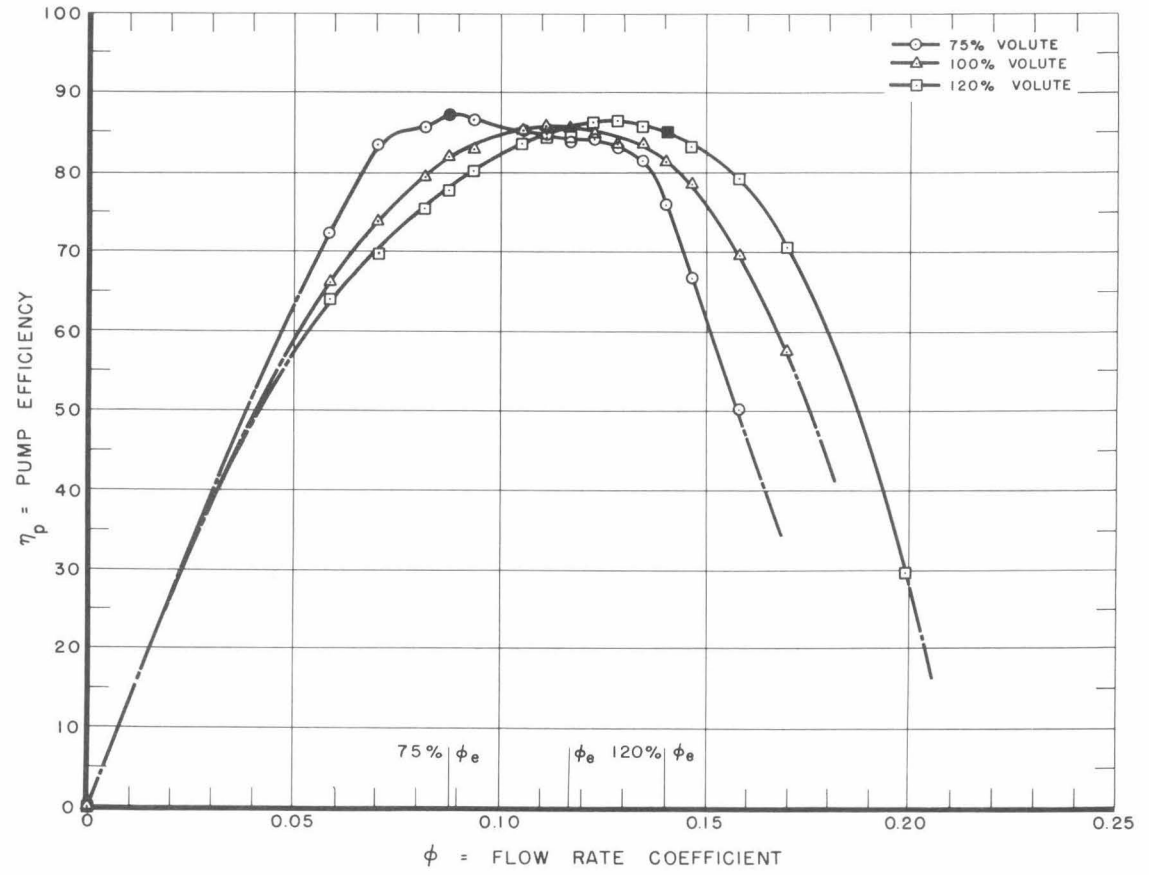

Fig. 16 - Pump efficiency for the three impeller-volute combinations.

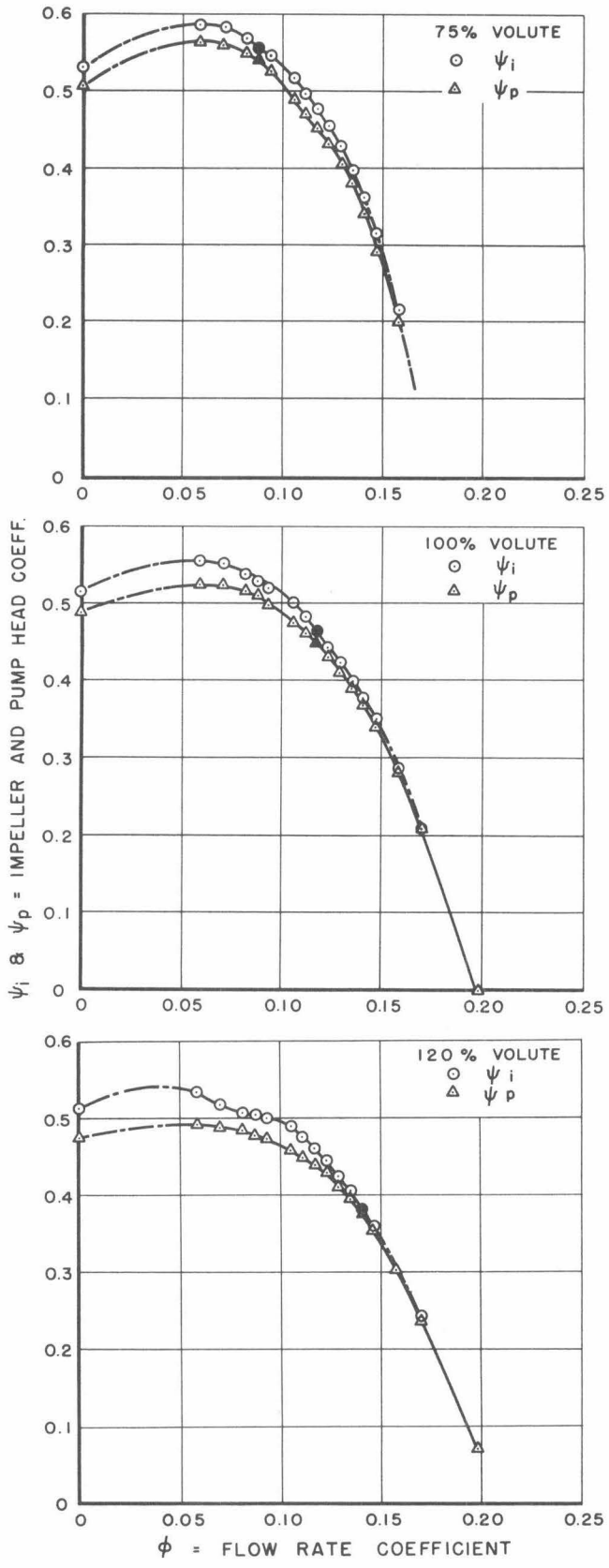

Fig. 17 - Impeller and pump head coefficients compared for the three volute shapes.

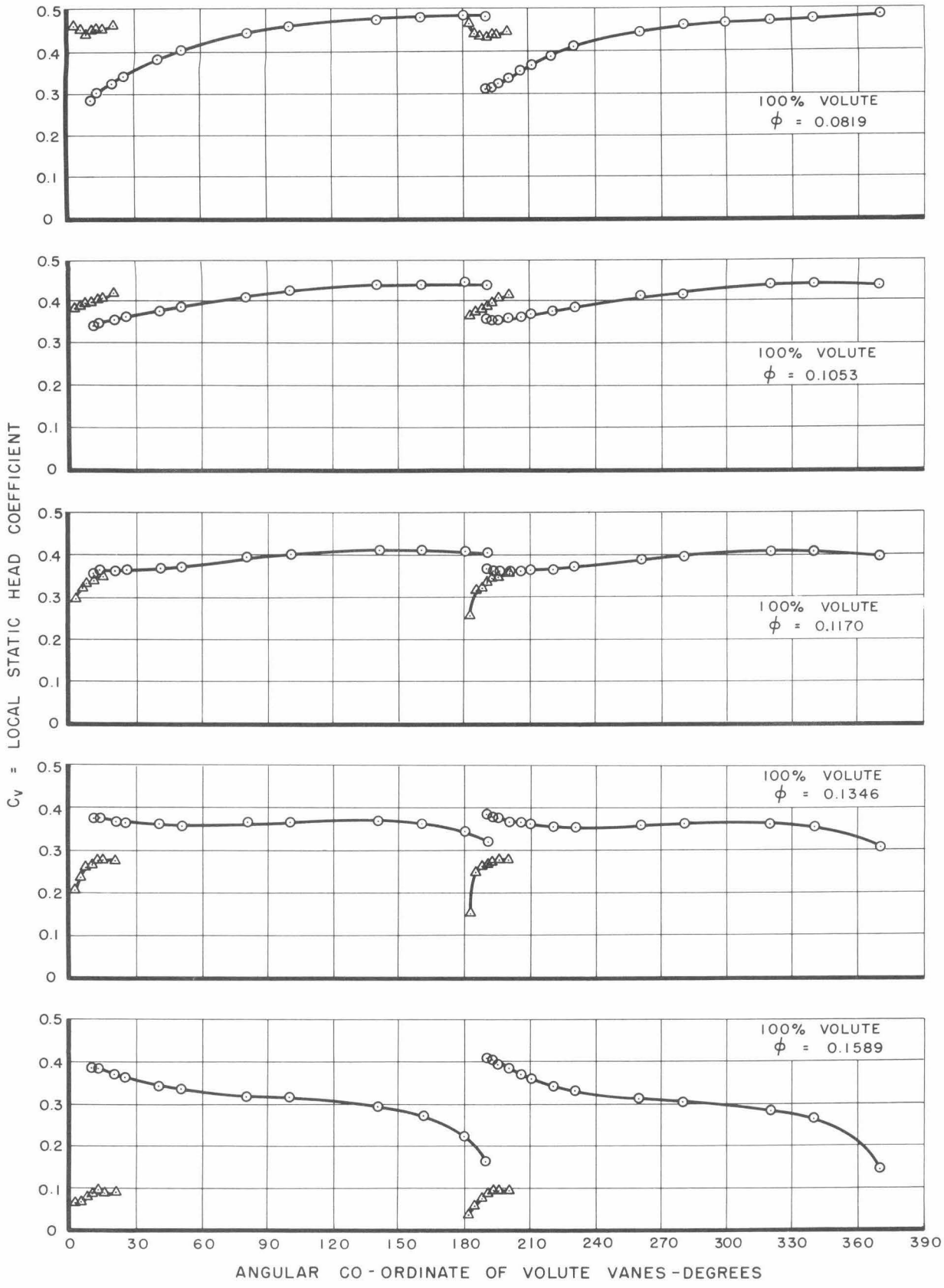

Fig. 18 - Volute vane static head distribution for the 100% volute.

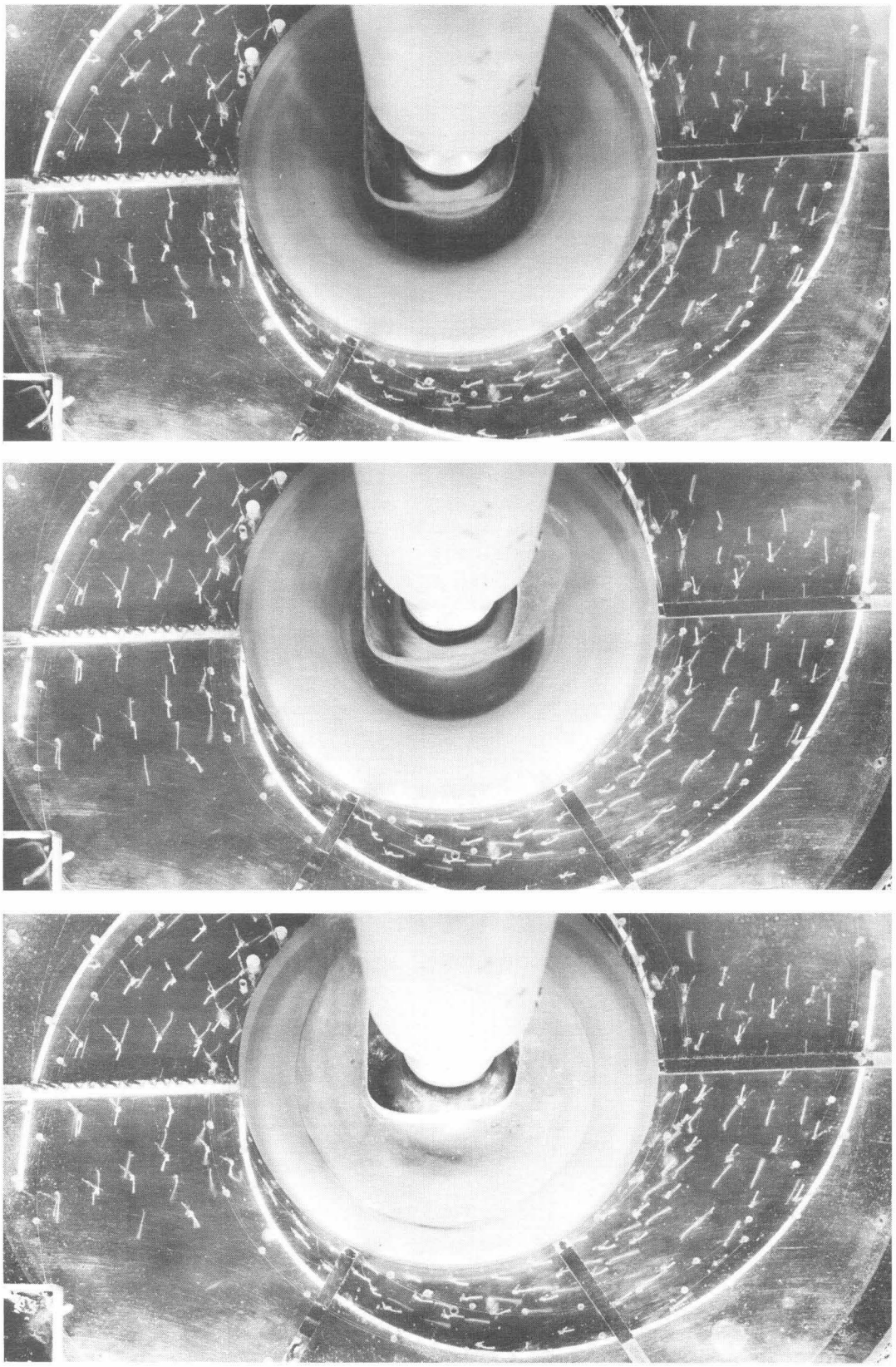

Fig. 19 - Streamer flow patterns in the 100% volute. Short streamers 1/2" from bottom shroud; long streamers on bottom.

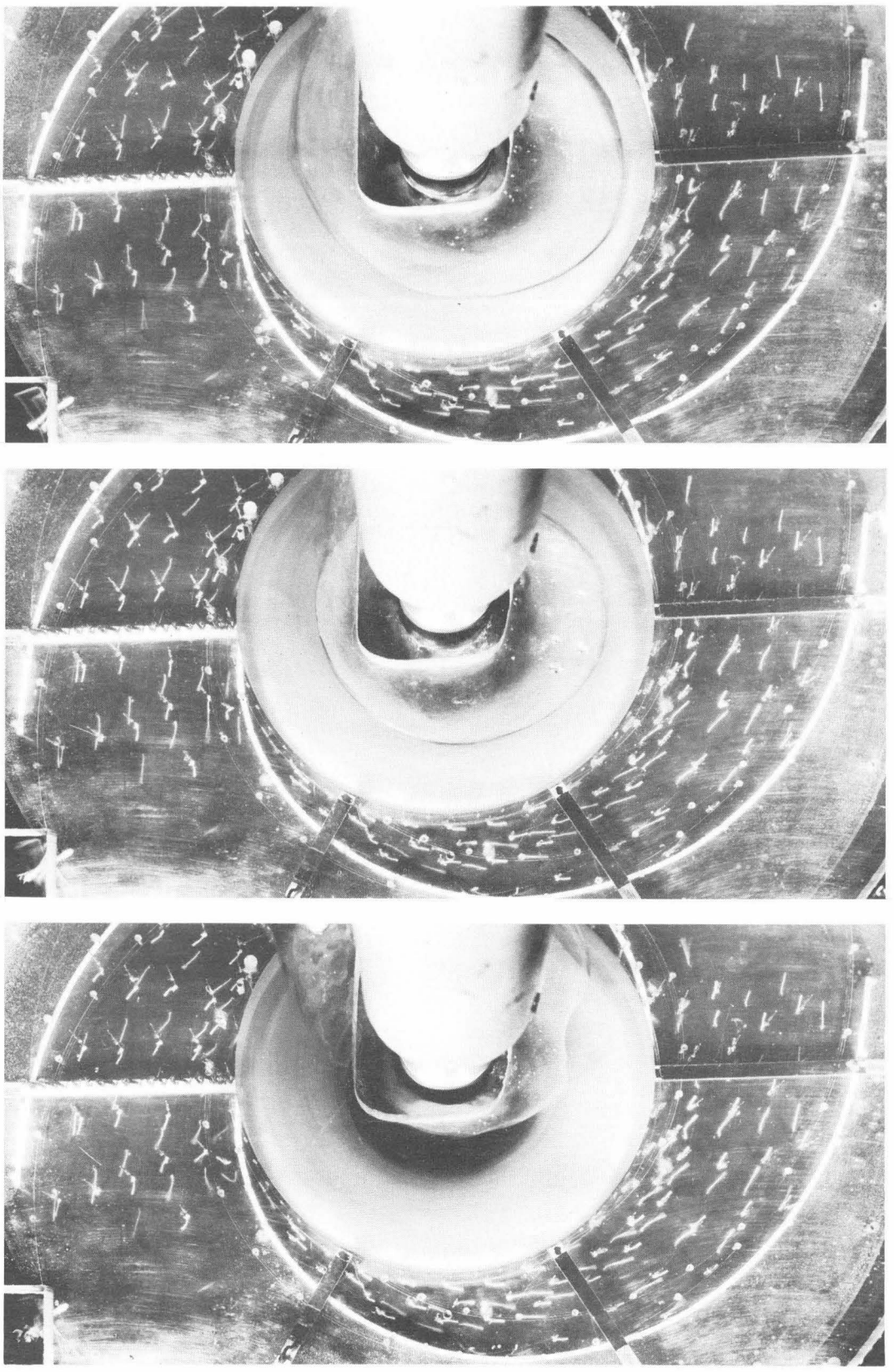

Fig. 19 (concluded) - Streamer flow patterns in the 100% volute. Short streamers 1-1/16" from bottom shroud; long streamers on bottom.